Google LLC
25 Massachusetts Avenue NW
Ninth Floor
Washington, DC 20001

202-346-1100 main
google.com

June 8, 2018

Via Electronic Filing

Marlene H. Dortch
Secretary
Federal Communications Commission
445 Twelfth Street SW
Washington, DC 20554

Re: *Request by Google LLC For Waiver of Section 15.255(c)(3) Of the Commission's Rules (ET Dkt. No. 18-70)*

Dear Ms. Dortch:

As anticipated in Google's reply comments[1] on its petition seeking waiver of Section 15.255(c)(3) of the Commission's Rules[2] to allow for certification of devices containing Project Soli sensors at power levels consistent with European Telecommunications Standards Institute (ETSI) standard EN 305 550,[3] Google here supplements the record with additional data demonstrating Soli sensors' ability to coexist with 802.11 technologies in the 60 GHz band. We

---

[1] *See* Reply Comments of Google LLC In ET Docket No. 18-70 at 2 (filed Apr. 23, 2018) (Google Reply Comments).

[2] *See* Request by Google LLC For Waiver of Section 15.255(c)(3) of the Commn's Rules in ET Docket No. 18-70 (filed Mar. 7, 2018) (Petition).

[3] *See* ETSI, *Electromagnetic Compatibility and Radio Spectrum Matters (ERM); Short Range Devices (SRD); Radio Equipment to be Used in the 40 GHz to 246 GHz Frequency Range; Part 2: Harmonized EN Covering the Essential Requirements of Article 3.2 of the R&TTE Directive*, ETSI EN 305 550-2 V1.2.1 (Oct. 2014), *at* http://www.etsi.org/deliver/etsi_en/305500_305599/30555002/01.02.01_60/en_30555002v010201p.pdf (EN 305 550). An update to EN 305 550 including the same power levels is expected to be cited in the Official Journal of the European Union by November 2018. *See* ETSI, *Short Range Devices (SRD); Radio Equipment to be Used in the 40 GHz to 246 GHz Frequency Range; Harmonised Standard for Access to Radio Spectrum*, EN 305 550, V2.1.0 (Oct. 2017), *at* http://www.etsi.org/deliver/etsi_en/305500_305599/305550/02.01.00_20/en_305550v020100a.pdf; ETSI, *Work Programme*, *at* https://portal.etsi.org/webapp/workProgram/Report_Schedule.asp?WKI_ID=46714. While Soli devices presently in development would not operate at the maximum power levels permitted in EN 305 550, grant of Google's waiver request would offer flexibility for future innovation in Soli technology, while complementing previous Commission action to promote harmony and keep pace with international standards. *See* Petition at 4.

also discuss below the reasons why Soli-based devices will not cause harmful interference to protected remote sensing satellite equipment.

Coexistence with other unlicensed devices.[4] First, in response to comments received on the Petition, Lovefield Wireless on behalf of Google prepared a supplement to its initial simulation study,[5] which is provided as Attachment A. In response to critiques[6] that most Wi-Fi consumer devices at 60 GHz use Single Carrier modulation rather than Orthogonal Frequency-Division Multiplexing (which assertedly has better receive performance when subject to narrowband interference), the supplemental Lovefield Wireless analysis models Single Carrier modulation and coding schemes of 60 GHz Wi-Fi. The supplemental analysis also accounts for the effects of Soli's duty cycling on its interaction with Wi-Fi. Additionally, the analysis provides calculations using a non-line-of-sight path loss channel model from the IEEE 802.11ad standard as well as the original free space line-of-sight channel model. Finally, the analysis examines outlier scenarios discussed by some commenters,[7] particularly the situation in which Soli devices and Wi-Fi stations are positioned in extremely close proximity.

Consistent with the initial study's findings, the supplemental analysis concludes that Soli technology operated under the requested waiver will have little impact on Wi-Fi performance. Due to duty cycling, Soli is not active most of the time.[8] Even when Soli is active, it operates outside of a 60 GHz WiFi channel approximately 75% of the time. Lovefield Wireless took this into account in its work. In the vast majority of simulations generated by Lovefield Wireless, Soli creates only minimal interference, regardless of the power level at which Soli operates (-10 dBm, 7 dBm, or 10 dBm) and regardless of the duty cycle assumed for Soli (either 10% or even a theoretical 100%). The percentage of cases in which there is degradation in Wi-Fi throughput is always quite small (i.e., approximately 8% when the analysis uses the purely conjectural assumption that the Soli technology would act at 100% duty cycle) and negligible when Soli is duty cycled at 10%.

Lovefield Wireless additionally simulated an atypical scenario in which Soli technology was always in close proximity to the Wi-Fi client with the Wi-Fi access point farther away, rather than being placed randomly with respect to the Wi-Fi devices as would be expected in normal use. In that artificial worst-case scenario, there still were no negative effects on Wi-Fi throughput with a

---

[4] Google addressed arguments raised in the docket about in-device co-existence in its reply comments, explaining that its waiver request only would apply to devices for which Google is the responsible party under the Commission's device authorization rules. *See* Google Reply Comments at 6.

[5] *See* Dr. Stefan Mangold, Lovefield Wireless GmbH, *Assessing the Interference of Miniature Radar on Millimeter Wave 60 GHz Wi-Fi* (Feb. 21, 2018) (attachment to Petition).

[6] *See* Comments of IEEE 802 in ET Docket No. 18-70 at 2 (filed Apr. 11, 2018) (IEEE 802 Comments); Reply Comments of NCTA – The Internet and Television Ass'n in ET Docket No. 18-70 at 3 (filed Apr. 23, 2018).

[7] *See, e.g.,* Comments of Facebook, Inc. in ET Docket No. 18-70 at 1 (filed Apr. 11, 2018); Reply Comments of Facebook, Inc. in ET Docket No. 18-70 at 2 (filed Apr. 23, 2018).

[8] Even the nominal 10% duty cycling figure used in the simulation studies is conservative. In normal steady state, Soli's duty cycle is less than 1%. Only when the Soli technology perceives that a gesture is being made does its duty cycle briefly increase, but only to a level of less than 10%. This duty cycle is sufficient for Soli's applications, and operating in excess of this duty cycle could needlessly deplete battery life.

Soli transmit duty cycle of 10%. Even when the analysis used the theoretical duty cycle of 100% for Soli technology operating in close proximity to the Wi-Fi, the simulations showed no harm to Wi-Fi throughput 80% to 95% of the time.

To check the reliability of the simulation studies conducted by Lovefield Wireless, Google took laboratory measurements of actual interference between a Project Soli device and commercially available IEEE 802.11ad equipment. A report describing the results of that controlled testing is provided as Attachment B. The laboratory measurements validate the main conclusion of the Lovefield Wireless simulations. Namely, for Soli technology to cause significant harmful interference to an 802.11ad link, the Soli sensor has to be positioned directly between the 802.11ad client and access point, with the Soli antenna transmitting from a position extremely close (i.e., within a few inches) to and directly into one of the 802.11ad antennas. This positioning is improbable in the real-world[9]. Furthermore, notably, an 802.11ad link is degraded to a lesser degree by a Soli device placed in close proximity to it than it is by a second 802.11ad link in close proximity—a scenario that is much more likely in the real world.[10] In that regard, commenters expressing concern about harmful interference may not realize that Soli is a gesture-sensing technology intended to face the user with a conical antenna pattern, and thus it generally will not be active unless in a user-facing position. As a result, Soli is unlikely to be active when its antenna is pointing directly at an 802.11ad antenna with little space between them.

Both the simulation studies and laboratory measurements provided in support of Google's Petition thus demonstrate that, at the intended power levels, Soli technology will cooperatively share 60 GHz spectrum with other unlicensed communications technologies. In general, the highly directional nature of 60 GHz devices lends itself to different technologies successfully sharing this spectrum. Moreover, Soli's low EIRP (which is more than 20 dB below that authorized for communications devices in the Commission's rules),[11] fast sweep cycle across frequencies during active transmissions, and proportionately long periods of inactivity allow equitable sharing with other communications technologies–even in the unlikely case of close proximity together with antenna alignment. As noted in the Petition, since 2014, ETSI standard EN 305 550 has allowed sensors and other technologies to transmit at higher power levels than the Commission's rules currently allow, and interference with unlicensed communications technologies has not been raised as a concern in geographies where such devices are free to operate.

[9] Notably, concerns that Soli technology could interfere with 802.15.3e as a near-proximity communications standard are even less likely to materialize than for 802.11ad, because intended range for 802.15.3e is 10 cm or less, which is much shorter than for 802.11ad. *See* Attachment B at 11, n.1.

[10] *See* IEEE 802 Comments at 1 (stating that Listen Before Talk in 802.11ad devices could mitigate interference between two 802.11ad devices in close proximity).

[11] *See* 47 C.F.R. § 15.255(c)(1)(i) (limiting the average power of any emission to 40 dBm and the peak power of any emission to 43 dBm for communications devices).

Coexistence with EESS. Likewise, concerns raised in the record about potential effects of airborne use of Soli-based devices on remote sensing satellite equipment are misplaced.[12] Attachment C to this letter is a study demonstrating the compatibility of airborne use of Soli devices with spaceborne Earth Exploration-Satellite Service (EESS) sensors. The study uses very conservative assumptions about Soli devices likely to operate under the requested waiver and their operating characteristics. Even under these assumptions, the results show that the potential for widespread airborne use of Soli would protect existing EESS sensors with a margin of at least 34 dB. The study also includes a worst-case analysis examining potential future EESS sensors whose specific operating characteristics are not known and shows a likely interference margin of at least 22 dB.

These analyses collectively confirm that the Commission should expeditiously grant Google's Petition. Unlicensed devices like Project Soli must share spectrum in the 60 GHz band cooperatively among themselves,[13] and "must not cause harmful interference to authorized services."[14] Project Soli technology meets these standards and can operate harmoniously with protected operations and unlicensed devices in the band. Furthermore, granting the Petition would "encourage the provision of new technologies and services to the public" consistent with Section 7 of the Communications Act of 1934,[15] thus promoting the public interest. Grant of the Petition also would serve the Commission's intent in modifying Rule 15.255(c)(3) to allow radars to "detect hand gestures very close to a device to control the device without touching it," as well as its efforts to harmonize its regulations and keep pace with global standards.[16]

Because operation of Project Soli technology is unlikely to significantly degrade the performance of other unlicensed devices and will not negatively impact remote sensing satellite equipment, Google respectfully requests that the Commission expeditiously grant its Petition to

---

[12] Comments of Nat'l Acad. of Sci.'s Comm. on Radio Frequencies in ET Docket No. 17-80 at 6-8 (filed Apr. 20, 2018) (CORF Comments). Google's reply comments addressed concerns about airborne use of Soli technology raised by the National Radio Astronomy Observatory (NRAO), which were later echoed in reply comments by the Frequency Allocations in Remote Sensing (FARS) Technical Committee of the IEEE Geoscience and Remote Sensing Society. *See* Google Reply Comments at 2-5; Reply Comments of FARS Technical Comm. of the IEEE Geoscience and Remote Sensing Soc'y in ET Docket No. 18-70 (filed Apr. 23, 2018).

[13] *See In the Matter of Terrestrial Use of the 2473-2495 MHz Band for Low-Power Mobile Broadband Networks,* Report and Order, 31 FCC Rcd. 13801, ¶ 29 (2016) (the Commission has underscored on many occasions that "unlicensed devices operate under the fundamental condition that they are not protected against harmful interference."). *See also* Julius Knapp, Chief, OET, FCC, *Industry Makes Progress on Unlicensed LTE Coexistence* (Sept. 23, 2016), *at* https://www.fcc.gov/news-events/blog/2016/09/23/industry-makes-progress-unlicensed-lte-coexistence (in the LTE context, the industry created standards including Wi-Fi, Bluetooth, and Zigbee within the FCC's regulatory framework for cooperative sharing of "spectrum by unlicensed devices while recognizing that such devices are not protected from interference.").

[14] *See In the Matter of Promoting Spectrum Access for Wireless Microphone Operations, et al.*, Order on Reconsideration and Further Notice of Proposed Rulemaking, 32 FCC Rcd. 6077, ¶ 6 (2017).

[15] *See* 47 U.S.C. § 157(a).

[16] *See In the Matter of Use of Spectrum Bands Above 24 GHz For Mobile Radio Services, et al.,* Report and Order and Further Notice of Proposed Rulemaking, 31 FCC Rcd. 8014, ¶ 337 (2016).

enable certification, marketing, and effective operation of the Project Soli gesture-sensing technology at levels consistent with those in ETSI standard EN 305 550.

Respectfully submitted,

Megan Anne Stull
Counsel
Google LLC

ATTACHMENT A

Dr. Stefan Mangold
Lovefield Wireless GmbH, Switzerland
www.lovefield.ch
stefan.mangold@lfield.ch

Assessing the Interference of Miniature Radar on Millimeter Wave 60 GHz Wi-Fi — Supplemental Analysis

June-08, 2018

Summary

1. This document supplements a study that accompanied Google LLC's Request for Waiver of Power Levels for Project Soli filed at the Federal Communications Commission on March 7, 2018.
2. There are four main additions to the original simulation study. First, the Wi-Fi system model now specifically models the single-carrier modulation and coding schemes of 60 GHz Wi-Fi. Second, the study now accounts for the fact that the radar is out of band of the WiFi channel for 75% of the time that the radar is actively transmitting. Third, for increased refinement, a non-line-of-sight path loss channel model taken from IEEE 802.11ad standardization is used in addition to the original free space line-of-sight channel model. Fourth, an additional scenario is added in which the radar devices and Wi-Fi stations are positioned so that outlier circumstances such as close proximities between interferer and victim can be better identified.
3. After making these additions, the main findings are consistent with those of the first study:
   (i) For the typical indoor scenario and with both path loss channel models, the Wi-Fi throughput is only marginally affected by interference from the radar (around 10% throughput reduction and generally far less, if any at all).
   (ii) Radar duty cycling further helps the radar to efficiently coexist with 60 GHz Wi-Fi.
   (iii) In outlier short range scenarios with co-located devices in close proximity to each other, a radar interferer can create additional interference, but only during in-band operation, as duty cycling of the radar mitigates this effect.
   (iv) Simulated throughput results match laboratory measurements with commercially available IEEE 802.11ad equipment.

Table of Contents

1. Introduction

An earlier study (Mangold, 2018) analyzed the interference effects of a radar system on 60 GHz Wi-Fi. This supplementary analysis presents additional simulation results to provide further insights. Different kinds of 60 GHz Wi-Fi systems, with different channel models, and other scenario configurations are investigated by this supplemental analysis.

An extended Wi-Fi system model is introduced that contains the IEEE 802.11ad single carrier (SC) modulation and coding schemes (MCSs) (IEEE 802.11ad, 2014 and IEEE 802.11, 2016), in addition to the MCSs using Orthogonal Frequency-Division Multiplexing (OFDM) considered in the earlier study. Thus, Wi-Fi devices with SC MCS that were offered in the market earlier and are more likely to be commercially available are addressed.

The supplemental analysis also highlights short range scenarios with devices in close proximity to each other. These additional scenarios offer a better understanding of extreme cases (very short range, no duty cycle), independently of how likely or unlikely such scenarios are to actually occur.

The extended radar system model used for this supplemental study is refined by including a simple in-band time assumption, because approximately 75 % of the time the Continuous Wave (CW) radar will operate out-of-band of the Wi-Fi channel.

Finally, this supplemental study contains both a free space line-of-sight path loss channel model (as in the earlier study) and a non-line-of-sight model. Both path loss models are derived from simulation models taken from IEEE 802.11ad standardization documents (Maltsev et.al., 2008 and Maltsev et.al., 2010).

1.1. Purpose and Limitation of this Analysis

This study is intended to offer interference analysis detailed enough to advance discussions concerning spectral coexistence between radars and Wi-Fi at 60 GHz, while remaining simple enough to allow readers to understand and evaluate the full model. The models underlying the Monte Carlo simulations are based on standard link budget models that are typically used when designing wireless networks, to assess link qualities, or to evaluate spectral coexistence of radio networks. Some radio parameters, such as the effect of multipath propagation, are only approximated in the path loss channel models. Other system behavior parameters, such as protocols or algorithms for dynamic radio resource management (for example, IEEE 802.11 distributed coordination function, power control, link adaptation, dynamic channel selection), are omitted to retain the model's simplicity and because they lack relevance to the analysis. While an alternative modelling approach based on, for example,

ray-tracing or real life measurements, theoretically would be possible, it also could become cost-prohibitive and inefficient given the large number of interference configurations potentially covered by the simulation. To achieve statistical relevance, typically between 20'000 and 50'000 samples are required for one parameter distribution. Relevant implementation details can be found in the Appendix.

1.2. Document Outline

The channel model used in this study is described in Section 2.

Section 3 describes the study's detailed model of the IEEE 802.11ad SC MCS. This section contains a basic evaluation of the theoretical performance of IEEE 802.11ad SC MCS, given the system model and channel model assumptions taken herein. This performance analysis does not analyze interference from radars.

Section 4 contains the description of how the narrow-band continuous wave radar interference and its effect on Wi-Fi are modelled. The simulation results that analyze the interference are presented and discussed in Section 5.

Section 6 contains a brief model validation and a comparison of the simulation results to laboratory measurements.

Section 7 concludes with final remarks, followed by a list of references.

The Appendix contains an erratum to the study that accompanied Google LLC's Request for Waiver of Power Levels for Project Soli filed at the Federal Communications Commission on March 7, 2018. The Appendix also provides implementation details of the simulation model used herein.

2. Path Loss Channel Model

In coexistence studies, simulation results depend on the accurate assessment of signal and interference power levels measured at the antenna of a victim radio station. Distance-dependent signal attenuations are modelled with a simple path loss approximation. An empirically derived path loss model, intended to assist simulation studies of IEEE 802.11ad, can be found in Maltsev et.al. (2009). A number of scenarios are defined in Maltsev et.al. (2009), for which the path loss model parameters are modified to match real life propagation characteristics. Two of the scenarios are used in this study: "*Living Room, LOS*" and "*Living Room, NLOS.*" Maltsev et.al, (2009).

Equation 1 describes the model of the simulation study. The reference distance chosen is 0.5 meters, below which no change of signal attenuation when compared to the reference distance is taken into account. This is a common solution to approximate short distance attenuations close to the antenna near fields (Rappaport, 2008).

Table 3 summarizes parameter values. Figure 1 illustrates the resulting signal to noise ratios in the absence of radar interference, which is analyzed later in this document. For simplicity's sake, shadow fading variations, as proposed for NLOS in the original sources, are not taken into account (zero standard deviation) during simulation.

Link budget models include gains of the transmitter and receiver antennas. The antenna gain depends on the antenna's direction. In this study (if not otherwise defined), it is assumed that the radar antenna points to an arbitrary, randomly chosen direction in azimuth that changes with each experiment. The Wi-Fi transmitter antenna at the access point and the receiver antenna at the station are assumed to be identical and directed towards each other. There is no third dimension, i.e., no modelling of signal emissions in elevation. See Figure 2 for an illustration of the antenna patterns.

$$PL[dB] = A + 20 \cdot \log_{10}\left(\frac{f_c}{1\,Hz}\right) + \begin{cases} 10 \cdot n \cdot \log_{10}\left(\frac{r}{1\,m}\right) & \text{for } r \geq 0.5\,m \\ 10 \cdot n \cdot \log_{10}\left(\frac{1}{2}\right) & \text{for } r < 0.5\,m \end{cases} \qquad \textbf{(Equation 1)}$$

Model	f_c [GHz]	A [dB]	n	Std. Dev. Shadow Fading
LOS	60.48	32.5	2.0	0
NLOS	60.48	44.7	1.5	0

Table 1: Path loss model parameters.

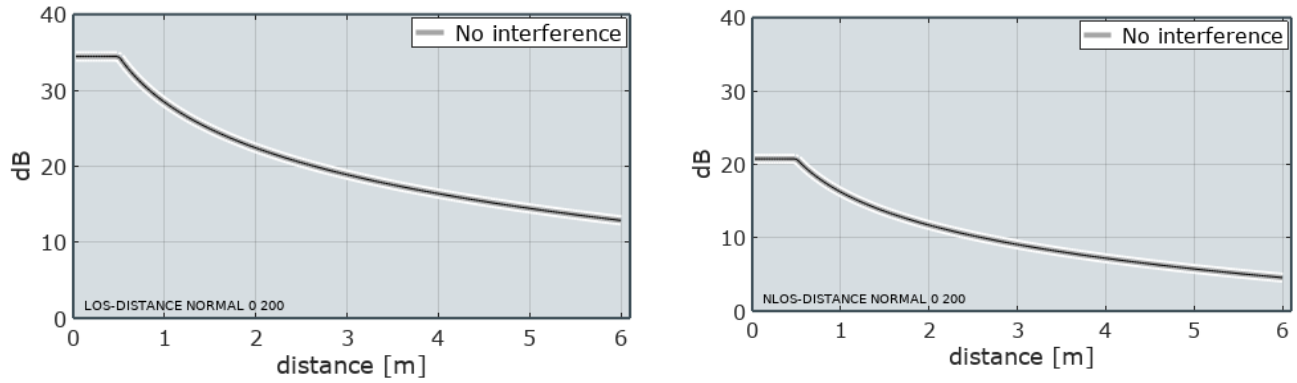

(a) LOS (b) NLOS

Figure 1: Signal to noise (Eav/N0) ratio over distance between radio devices (Wi-Fi or radar) for two channel models. The effect of the reference distance (0.5 m) and the influence of parameter A in both models can be observed.

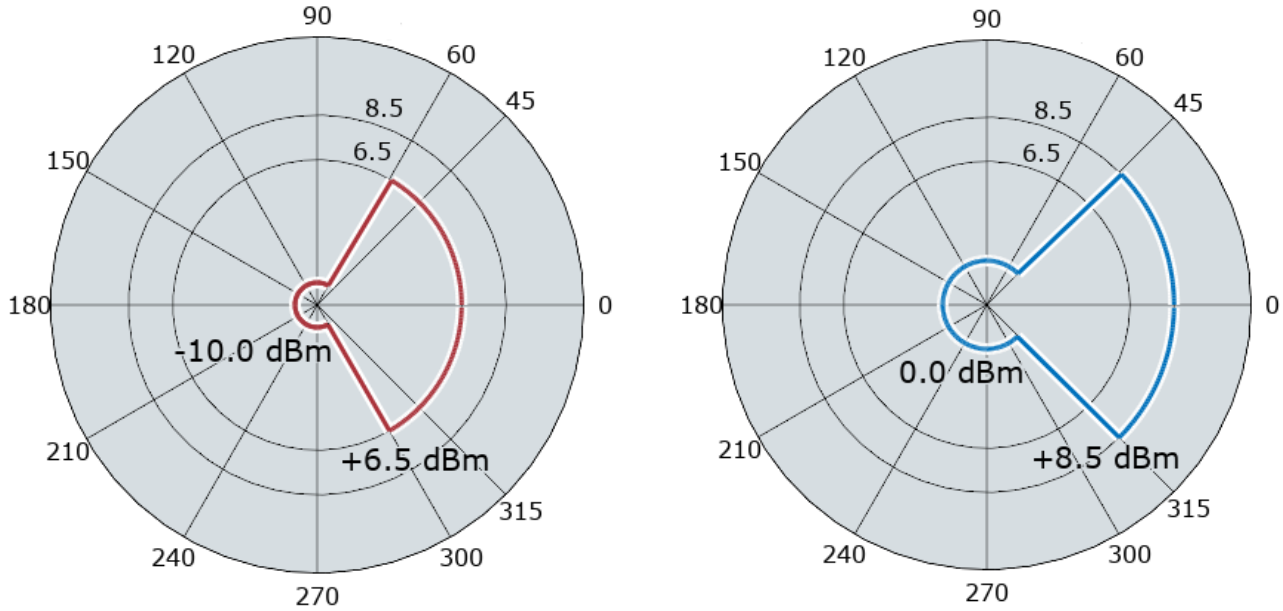

(a) Radar transmitter antenna (b) Wi-Fi transmitter and receiver antenna (90 degree angle, four antenna sectors).

Figure 2: Radar and Wi-Fi 2-D antenna patterns as used in the simulation. Wi-Fi 60 GHz antennas operate with antenna sectors. The 90 degree beam angle indicated in Figure (b) leads to four antenna sectors. The number of sectors available to a station depends on the directionality of the station's antenna, and is increased by increasing the number of antenna elements that are deployed in a station. Nitsche et.al. (2014) claim that 1 … 32 elements are common in consumer devices such as smartphones, handheld devices, tablets or notebooks. Therefore, four antenna sectors (90 degree angle) are chosen here as a conservative approach to model most types of consumer devices. Note that the back-lobe gain of the Wi-Fi antenna is conservatively chosen to be quite large (0 dB), which makes the Wi-Fi device more vulnerable to interference in the study than is expected in practice.

3. 60 GHz Wi-Fi Single Carrier Model

This section describes the mathematical model of the 60 GHz Wi-Fi system used in this study. Section 3.1 summarizes the system parameters. Section 3.2 describes the model and contains figures showing the theoretical performance in the presence of thermal noise (without any radar interference).

3.1. 60 GHz Wi-Fi with Single Carrier (SC) Modulation and Coding Scheme (MCS)

Whereas Mangold (2018) studies the 60 GHz Wi-Fi with OFDM multicarrier modulation, this study examines the impact of the radar on the SC Modulation and Coding Schemes (MCS 1 to MCS 12) of IEEE 802.11ad (IEEE 802.11ad, 2014 and IEEE 802.11, 2016).

Channel bandwidth and center frequency	2160 MHz | 60.48 GHz
Signal bandwidth (-17 dBr transmit mask)	1880 MHz
Symbol rate ("SC chip rate" in 802.11ad)	1760 MHz
Symbol duration ("SC chip time" in 802.11ad)	1/1760 MHz = 0.56818 ns
Modulation	**π/2-BPSK | π/2-QPSK | π/2-16QAM**
Physical layer bitrate (modulated, no coding)	1760.0 Mbps | 3520.0 Mbps | 7040.0 Mbps
LDPC code rate MCS 1	1/4 **(repetition, with code rate 1/2)**
LDPC code rate MCS 2 … 12	1/2, 5/8, 3/4, 13/16
LDPC code word size	672 bit
LDPC coding gain (approx.)	**Rate 1/4:** 8.0 dB | **1/2:** 6.0 dB | **5/8:** 4.0 dB **Rate 3/4:** 3.0 dB | **13/16:** 3.2 dB
Physical layer bitrate (LDPC encoded data)	440.0 Mbps **(MCS1)** … 5280.0 Mbps **(MCS12)**
Block size (BPSK | QPSK | 16-QAM)	448 bit | 896 bit | 1792 bit
Block duration (encoded data only)	254.55 ns
Golay sequence preceding each block	64 BPSK symbols (64 bit) | **duration:** 36.364 ns
Block duration (LDPC encoded data + Golay)	290.91 ns
Physical layer bitrate (LDPC encoded data + Golay)	385.0 Mbps **(MCS1)** … 4620.0 Mbps **(MCS12)**
Tx and Rx antenna beamform gain	8.5 dBi
Transmission peak power	**Used in this study:** 150 mW (21.76 dBm) EIRP **FCC limit:** 20 W (43.00 dBm) EIRP
Receiver implementation loss and noise figure N_f	15 dB

Table 2: 60 GHz Wi-Fi with SC modulation and coding schemes (mandatory MCS 1 … MCS 4, and the optional MCS 5 … MCS 12 in IEEE 802.11ad, 2014).

MCS	1	2	3	4	5	6	7	8	9	10	11	12
Sensitivity (1 % PER) [dBm]	-78	-68	-66	-65	-64	-62	-63	-62	-61	-59	-55	-54
Cut-off sensitivity $P_{rx,cutoff}$ (100 % PER) [dBm]	-81	-71	-69	-68	-67	-65	-66	-65	-64	-62	-58	-57

Table 3: 60 GHz Wi-Fi receiver sensitivities for MCS 1 to MCS 12. The sensitivities are defined in IEEE 802.11ad (2014) for levels that lead to a Packet Error Rate (PER) of 1 %. For the model, a cut-off sensitivity level is introduced and used.

Technical details of the SC MCS relevant to this study are given in Table 2 and Table 3. Figure 3 illustrates the operation in four frequency channels. Wi-Fi packets are assumed to be constructed with a number of consecutive SC symbols. This assumption leaves out special intervals such as ranging and synchronization phases, or transmissions with MCSs that are not SC.

In real life scenarios, Wi-Fi packet lengths depend on higher layer protocols and the payload size of the original data, and could vary significantly. The encoding also could change throughout the transmission of a Wi-Fi packet, from one symbol to the next, as some symbols that are required for reliable operation are transmitted at more robust and mandatory MCSs. All evaluations in this study assume operation on channel 2, which ITU-R recommends to be used as the default channel.

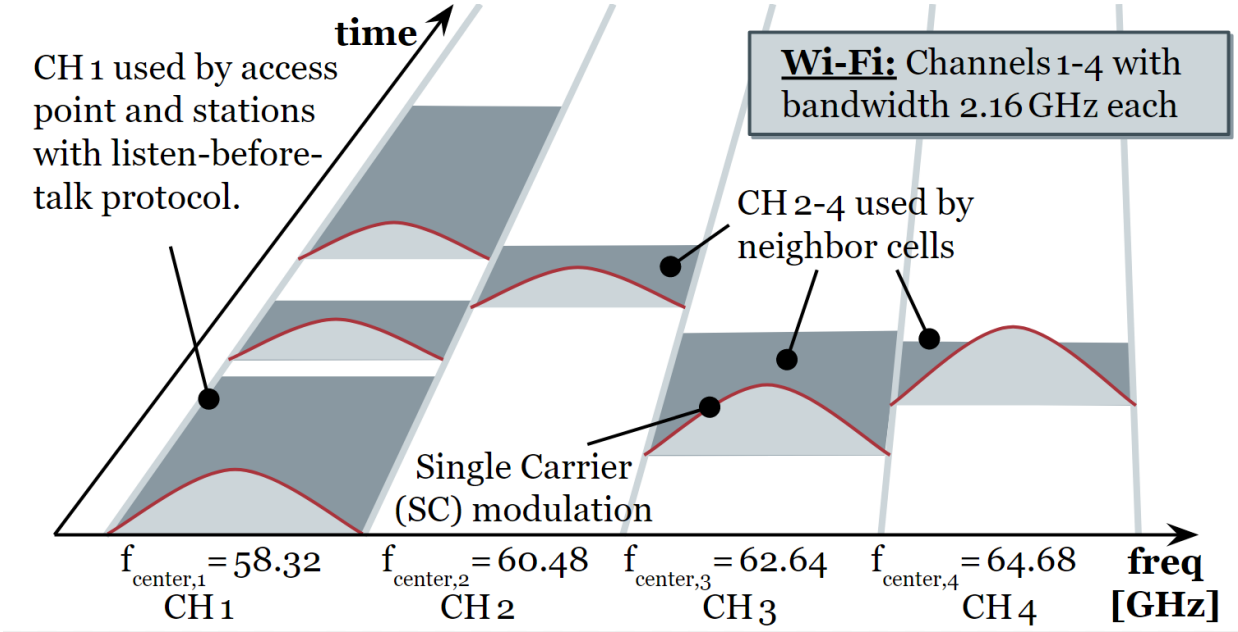

Figure 3: Radio spectrum access and frequency channels of 60 GHz Wi-Fi with SC modulation and coding scheme. Transmitted packets are based on a number of consecutive SC symbols. All evaluations in this study assume operation on channel 2, which ITU-R recommends to be used as default channel, because of its global availability.

3.2. SC Simulation Model

A Bit Error Ratio (BER) model for BPSK and quaternary modulation (QPSK, 16QAM) is applied to determine the code word error ratio and channel capacity in Wi-Fi. The results depend on the selected MCS. A Wi-Fi system typically adapts the MCS dynamically over time, for example to optimize the throughput in the presence of interference (link adaptation). This is included in the simulation model.

Parameter values are taken from Table 2 and Table 3.

3.2.1. Bit Error Ratio (BER)

The BER is given as a function of the Eav/N0 value, which is equivalent to the Signal-to-Noise Ratio.

$$\frac{Eav}{N0} = \frac{S}{N+I}. \qquad \textbf{(Equation 2)}$$

The symbol error ratio P_M for an M-ary QAM for the modulation index $M>2$ is given as

$$P_M = 1 - \left(1 - P_{\sqrt{M}}\right)^2. \qquad \textbf{(Equation 3)}$$

Equation 3 is valid for QPSK and 16QAM modulation, with

$$P_{\sqrt{M}} = 2 \cdot \left(1 - \frac{1}{\sqrt{M}}\right) \cdot Q\left(\sqrt{\frac{3}{M-1} \cdot \frac{Eav}{N0}}\right).$$

For QPSK and 16QAM modulation, the BER is approximated through

$$BER_{QPSK,\ 16QAM} = P_B^{(M)} \approx \frac{P_M}{\log_2(M)},\ M>2.$$

For BPSK modulation, the BER is approximated as

$$BER_{BPSK} = P_B^{(2)} \approx Q\left(\sqrt{2 \cdot \frac{Eav}{N0}}\right).$$

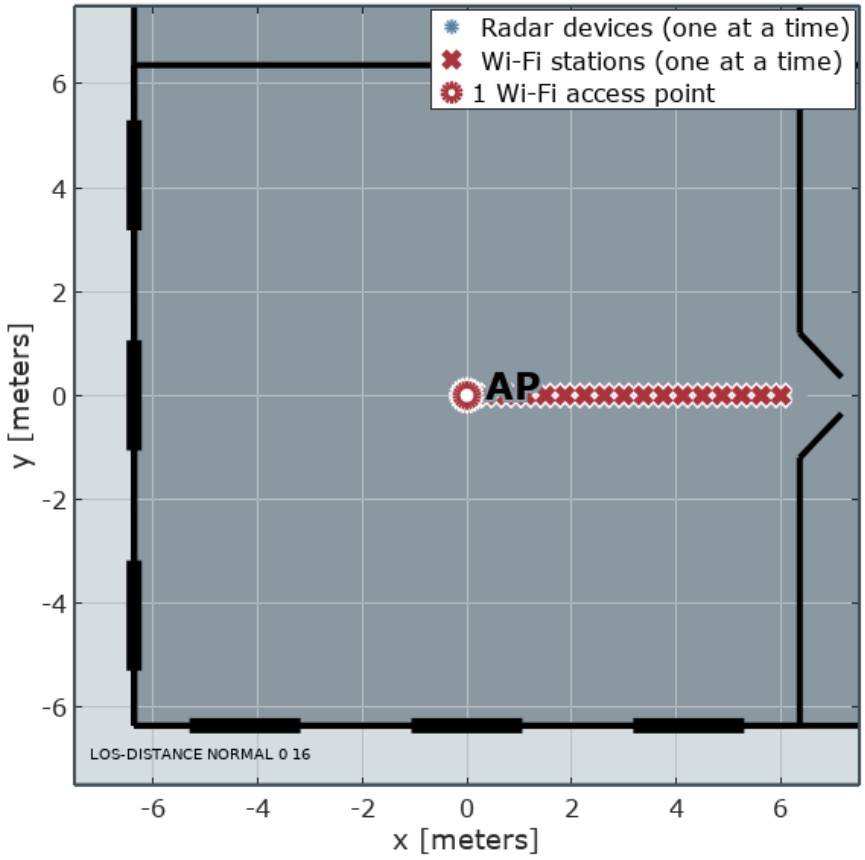

Figure 4: Scenario to demonstrate the performance of the SC MCS. Distances of up to thirty meters are evaluated.

3.2.2. Sensitivity

If the receiving Wi-Fi station is out of the transmitter's coverage range as defined by the cut-off sensitivity levels (Table 3), the BER is set to 100% to set the channel as highly unreliable:

$$BER = \begin{cases} BER & if\ P_{rx} > P_{rx,\,cutoff} \\ 1 & else \end{cases}$$

3.2.3. Code Word (Packet) Error Probability and Channel Capacity

The first-event bit error probability is taken into account. Assuming uncorrelated bit errors,[1] the codeword or Packet Error Ratio, PER, is given by

$$PER = 1 - (1 - BER)^{size\,(codeword)}$$

with code word size measured in *bit*. Table 2 defines the default size. Taking coding gains into account (low-density parity-check estimates as stated in Table 2), the resulting maximum channel capacity now can be defined.

It is affected by a constant overhead resulting from the periodic Golay sequences, and determined as

$$C = Codingoverhead \cdot (1 - PER) \cdot Rate \cdot GolayLoss\,.$$

3.3. Evaluation

The scenario shown in Figure 4 is used to evaluate the performance of the SC modulation. Results are shown over the distance between the transmitting Wi-Fi access point and the receiving Wi-Fi station. For both path loss models, LOS and NLOS, Figure 5 to Figure 9 show the BER, the code word error probabilities, the effect of the cut-off sensitivity level for all 12 MCSs, the resulting channel capacity for all 12 MCSs, and the Wi-Fi throughput obtained by selecting the optimal MCS mode to maximize the achievable Wi-Fi throughput. Radar interference is not included in the model. This is analyzed later in this document (Section 4: model, Section 5: results).

[1] The duration of a block (LDPC encoded data + Golay) is only 290.91 nanoseconds. Therefore, and because the channel model does not consider fading due to mobility or obstacles, it is assumed that the interfering radar signal will always affect all consecutive symbols within one code word (one block) similarly.

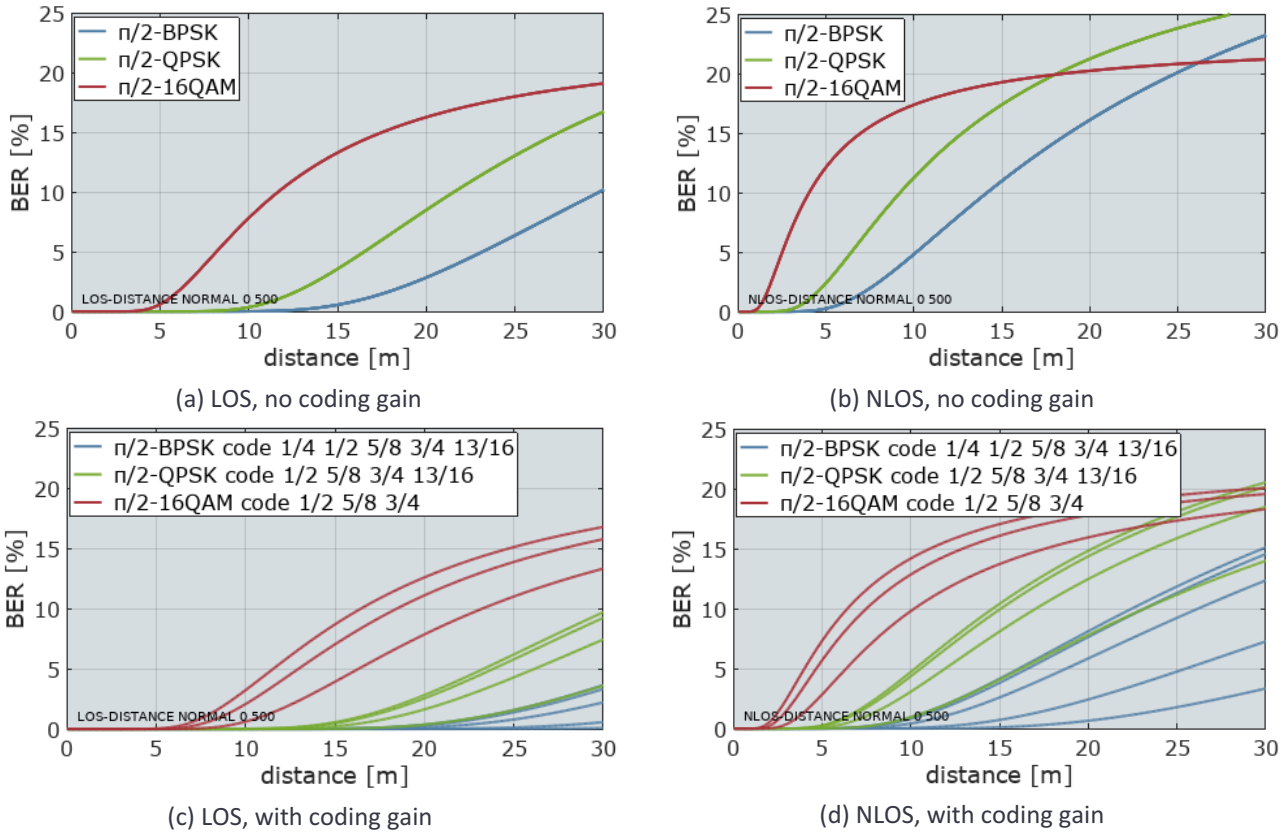

(a) LOS, no coding gain

(b) NLOS, no coding gain

(c) LOS, with coding gain

(d) NLOS, with coding gain

Figure 5: Theoretical Bit Error Ratio (BER) for the three modulations π/2-BPSK, π/2-QPSK, and π/2-16QAM. There is no radar interference. Only thermal noise is considered. Figures (a) and (b) show the theoretical BER for modulation without encoding. MCS 1-12 apply these three modulations by adding encoding. The estimated coding gains are taken into account by adding them to Eav/N0. The two bottom figures (c) and (d) indicate the theoretical BER when coding gains are considered.

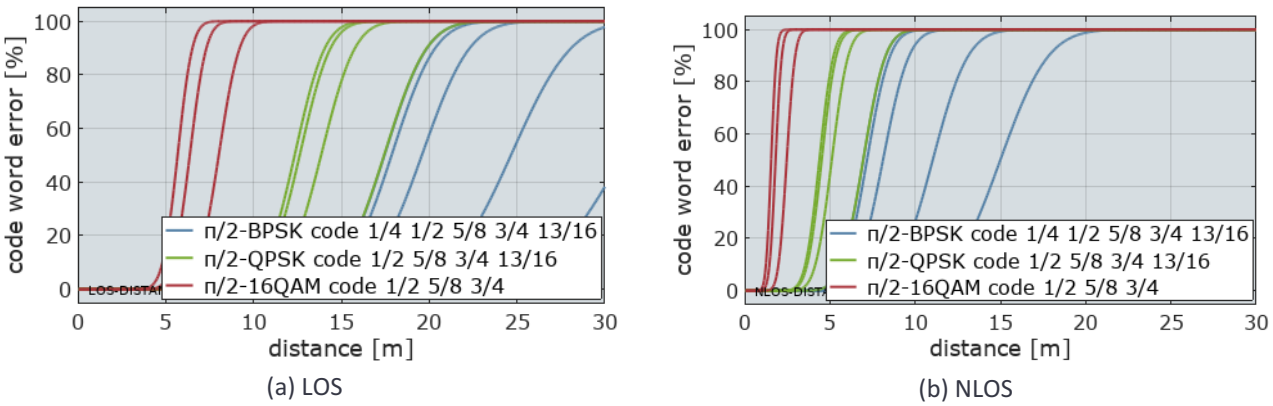

(a) LOS

(b) NLOS

Figure 6: Code word error probabilities for all MCSs, with coding gains.

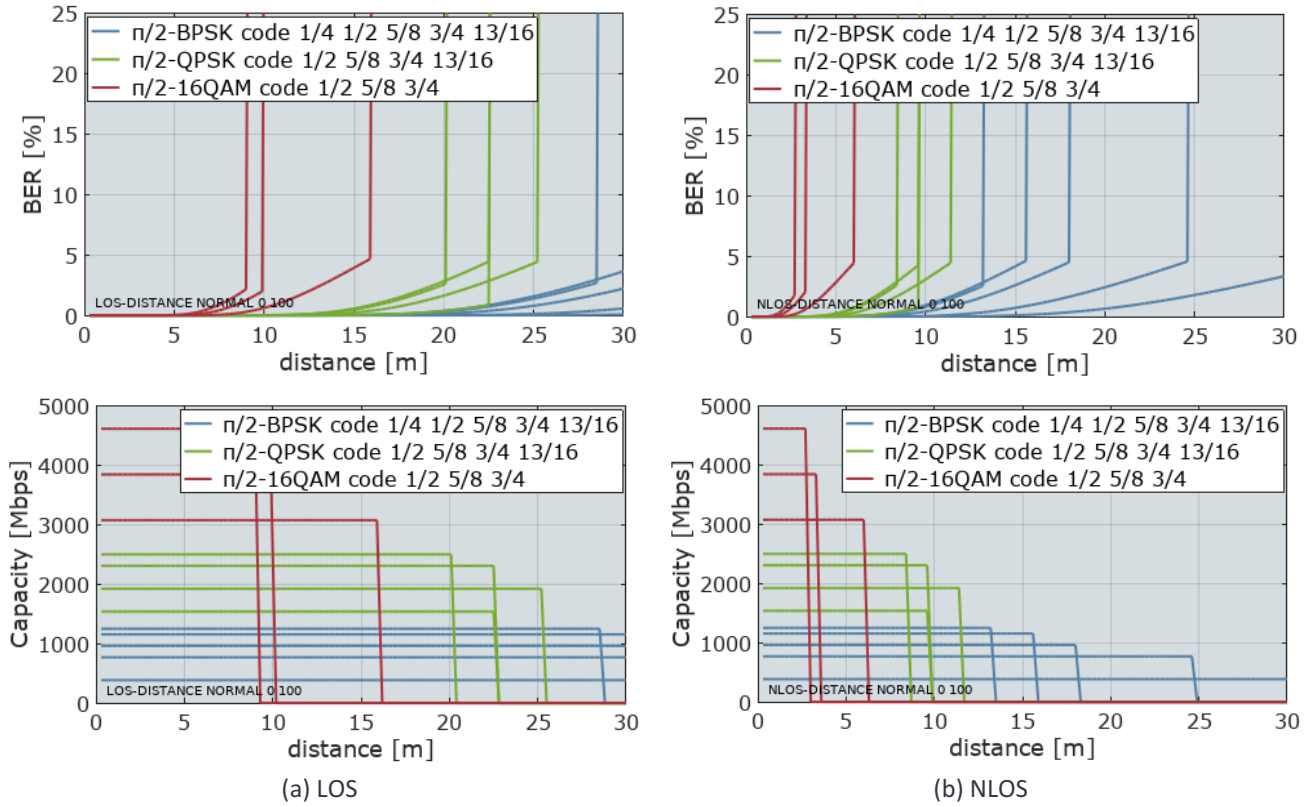

(a) LOS (b) NLOS

Figure 7: BER and capacity results including receiver sensitivity. The receiver sensitivity limits the coverage range of a radio system, but - given the path loss models applied here - this occurs at comparably large ranges.

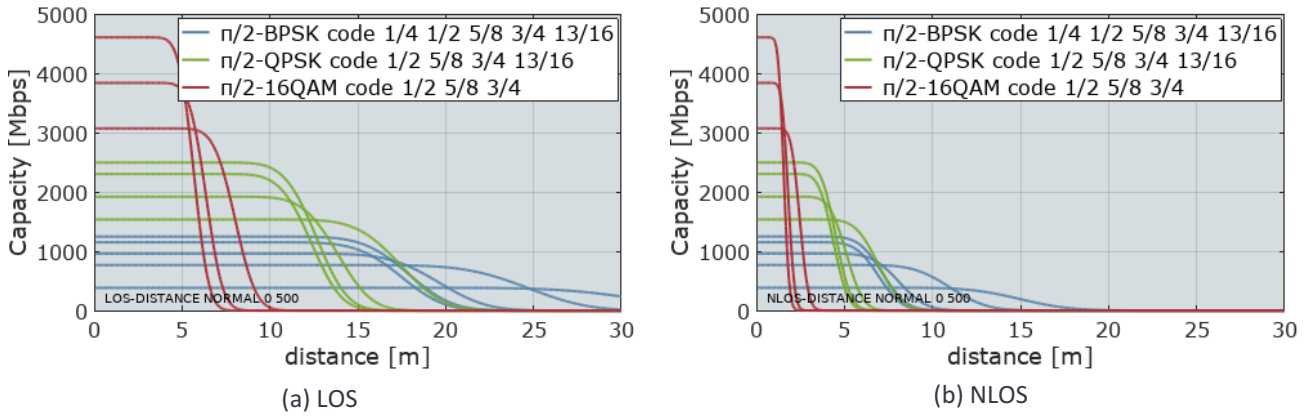

(a) LOS (b) NLOS

Figure 8: The resulting channel capacity for all twelve MCSs. One code word (size 84 byte) is used as packet size. There are no bit errors at short distances, and the capacity is only limited by coding overhead and Golay sequences. Different MCS modes achieve different maximum capacities. More robust MCSs trade the achievable capacity with an increased coverage range (distance). No radar interference, thermal noise only.

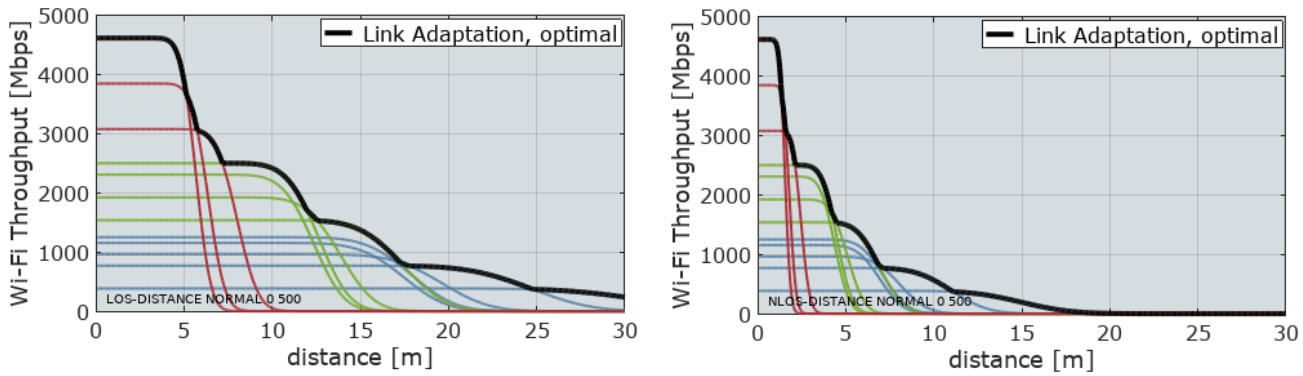

Figure 9: Wi-Fi applies dynamic MCS selection, also referred to as link adaptation. The resulting optimal Wi-Fi link throughput is indicated here. This dynamic MCS selection is the reason for the step-wise shape of some results in later sections. No radar interference, thermal noise only.

4. Interference Model

This section describes how the impact of continuous wave radar interference upon Wi-Fi SC modulation is modelled in this analysis. For the sake of clarity and conservatism, we employ a simplistic approach to modeling this interference, which in fact overemphasizes the effect of such interference on Wi-Fi.

As detailed in Mangold, 2018, the radar sweeps across 7 GHz over a duration of 600 us. As a result, the radar is transmitting within a Wi-Fi channel for approximately only 25% of that sweep time. These effects are illustrated in Figure 10 and Figure 11.

Given the slow speed of the radar sweep relative to the time for a single Wi-Fi symbol (~0.57 ns) or even a block (~290 ns), the radar is in effect a CW interference with constant frequency that is added to the SC modulated Wi-Fi waveform.[2]

The impact of such interference upon SC modulation is studied in detail in Axford (1992).[3] The effect of CW interference is understood by analyzing its effect upon the canonical matched filter-based receiver (at baseband). From first principles, the matched filter output (which at its core is an integration of the received waveform for a symbol period, or 0.57 ns here) is equal to the normal signal constellation plus additive Gaussian noise, plus an additional term equal to the integral of the CW interference over a symbol period. This is captured in Equations 8 and 10 of Axford (1992).

As a result, any CW interference shifts the received signal constellation by an offset. That offset is equal to the integration of the CW interference over the symbol period, and thus depends upon the frequency and phase of the CW interference relative to the Wi-Fi carrier frequency and the symbol timing boundaries, respectively.

[2] The analysis that follows makes it clear that the very small frequency shift that can occur from symbol-to-symbol and across blocks is not consequential, as the key is the radar interference energy that is integrated by the matched filter in each symbol.

[3] The analysis in Axford (1992) covers binary phase-shift keying (BPSK), and thus only considers the in-phase (I) component of the signal. However, the analysis can be extended to complex constellations (π/2-BPSK, π/2-QPSK, π/2-pi/2 16-QAM) in a straightforward manner by considering the matched filter output in both the in-phase (I) and quadrature (Q) components. Axford (1992) focuses on hard decoding of BPSK while Wi-Fi products are expected to employ the more powerful soft-decoding technique; however, degradation due to an increase in the effective noise level affects both hard- and soft-decoding in a similar manner. Axford (1992) also considers traditional SC modulation as opposed to the block-based (blocks of 512 symbols, including a 64-symbol Golay sequence) approach employed in 802.11ad; however, there is nothing inherent to the 802.11ad modulation structure that makes it more vulnerable to narrowband interference than the simpler system in the reference.

Based upon Equation 8 and Figure 6 of Axford (1992), it is evident that the CW interference has no effect (i.e., no shift of the constellation) when the interference is precisely at the edge of the Wi-Fi band, because in that case the CW interference spans its exact period in a Wi-Fi symbol period and thus integrates to zero. As the radar frequency approaches the Wi-Fi carrier frequency, its effect will increase (the integration will be over less than a symbol period of the sinusoidal interference, and thus almost always will be non-zero) and its impact will be maximal when the radar frequency is precisely at the Wi-Fi carrier frequency (again see Figure 6 of Axford, 1992). In this case, the signal constellation is shifted by the full amplitude of the interfering signal. As the radar frequency moves towards the upper end of the Wi-Fi band, its impact will again lessen.

Although the impact of the radar decreases substantially as the instantaneous radar frequency gets farther away from Wi-Fi's carrier frequency (see Figure 6 of Axford, 1992), for the sake of simplicity and in order to maximally model the impact of the radar on Wi-Fi, we assume that the impact of the radar on Wi-Fi (whenever it is in the Wi-Fi channel) is always worst-case, i.e., the frequency of the radar transmission is aligned with the Wi-Fi carrier. Under this counterfactual worst-case assumption, the signal constellation is shifted by a complex constant whose amplitude is equal to the amplitude of the interference (i.e., the square root of the interference power), with a phase determined by the relative phase of the interference (which can be modelled as uniformly distributed over all possible values) to the Wi-Fi carrier.

The final result is that the signal constellation is degraded by the standard thermal noise component (additive Gaussian noise), plus an additional term with random phase and amplitude equal to that of the interference. As is often done, and motivated by the worst-case nature of Gaussian noise,[4] the noise and the new additive term can be modeled by Gaussian noise with power equal to the sum of the thermal noise and the interference power.[5]

While this provides an accurate worst-case modeling of the interference that actually can be expected, in order to be even more conservative and conclusively address concerns regarding the impact of radar interference on Wi-Fi, we further boost the interference power in our analysis by a factor of 5 (i.e., 7 dB) before adding it to the thermal noise. This arbitrary adjustment of +7 dB is factored into throughput results provided later in this report.

[4] *See* Digavi and Cover (2001), and references therein.

[5] While thermal noise is indeed independent across successive data symbols, the additive component due to the radar interference may be correlated across symbols (because successive symbols experience the same sinusoidal interference, but integrated across successive and non-overlapping symbol time periods). The effect of such correlation is alleviated by the interleaving of information bits inherent in the LDPC-based forward-error correction implemented in 802.11ad. The +7 dB adjustment described at the end of this section provides further assurance that any lingering effects are captured by this study.

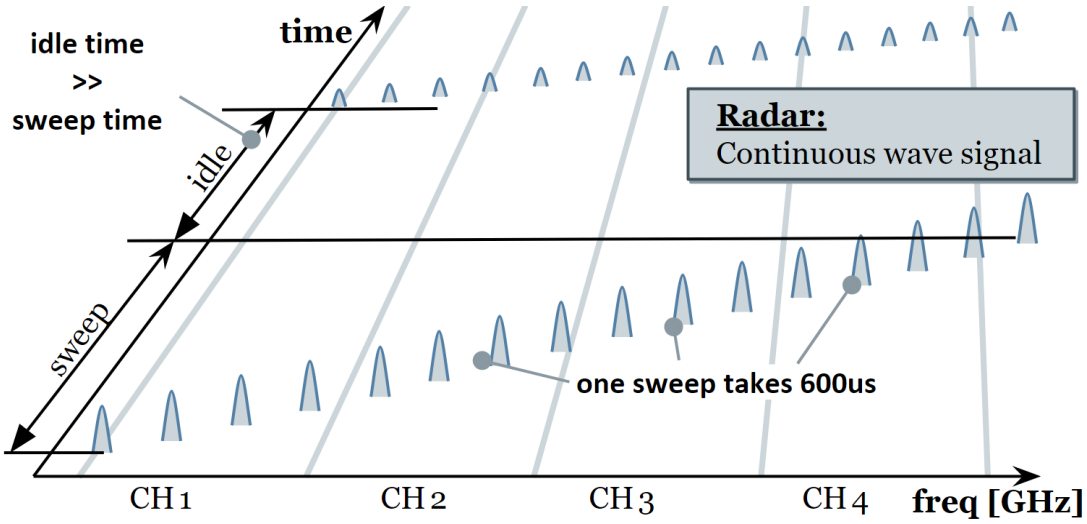

Figure 10: Timing of the radar signal. The idle time is determined by the duty cycle.

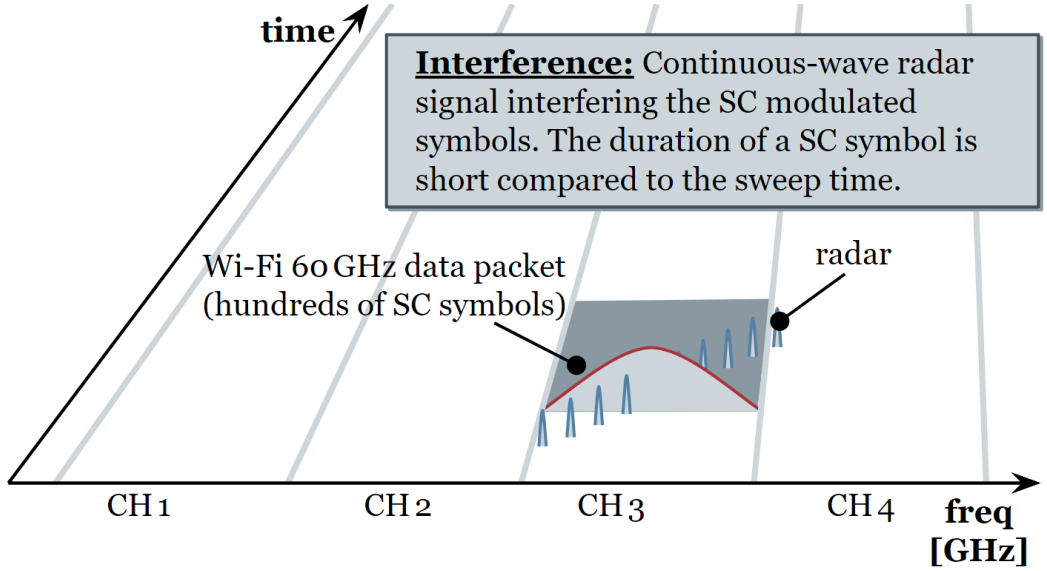

Figure 11: Interference calculation for SC modulation and coding scheme: The CW radar signal is modelled as interferer with random but time-invariant constant frequency offset (off-tuned) and random initial phase shift, during the duration of one SC symbol.

5. Simulation Results

All simulation results relevant to the interference scenarios are presented here. Two different scenarios are used to analyze the coexistence scenarios, see Figure 12.

(a) TYPICAL: Random locations for radar devices and Wi-Fi stations, covering all possible configurations. LOS and NLOS path loss models are used.

(b) SHORT_RANGE: Line of Wi-Fi stations with distances to the access point around half of the room width, with a radar interferer arbitrarily centered around the station, at short distance. Again, LOS and NLOS path loss models are used.

The simulation results presented in the remainder of this section (Figure 13 and Figure 14 for TYPICAL and Figure 15 and Figure 16 for SHORT_RANGE) focus on the same performance indicators as in the first study (received power, signal-to-noise ratio, channel capacity).

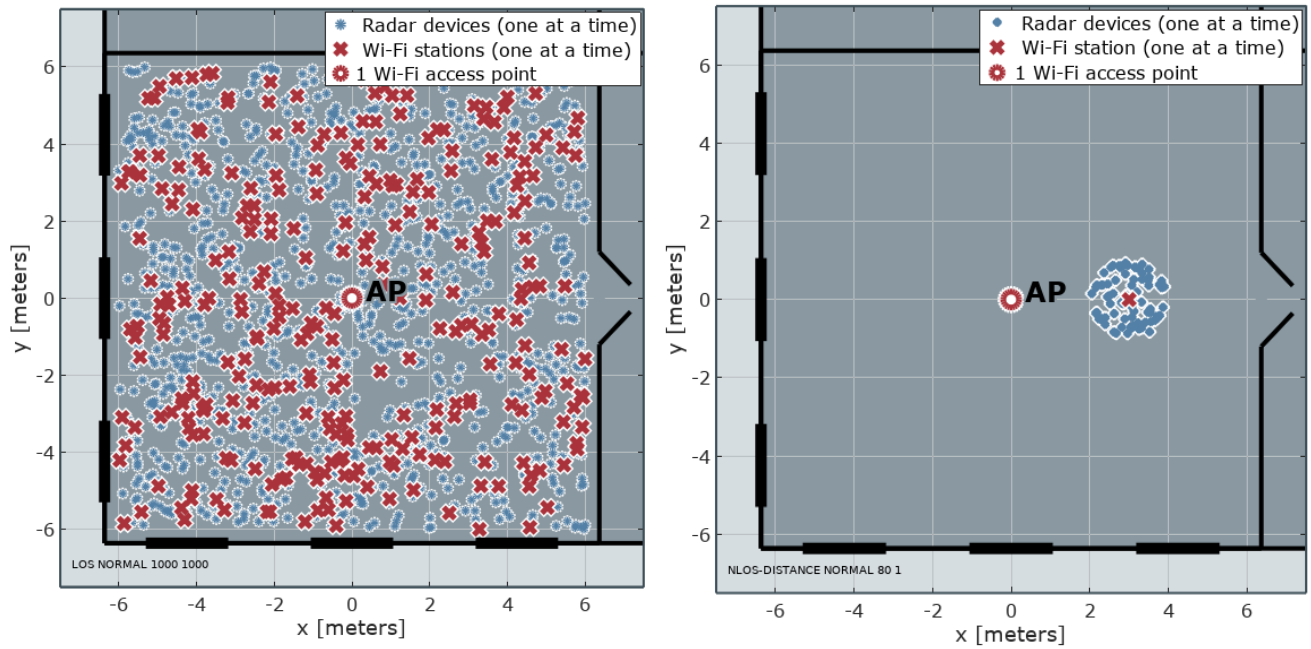

(a) "TYPICAL" with full room coverage. Channel model: LOS or NLOS.

(b) "SHORT_RANGE" Channel model: LOS or NLOS.

Figure 12: Simulation scenarios. There are always only three devices in each simulation experiment: One Wi-Fi AP, one Wi-Fi station, and one radar device. The Wi-Fi antennas always point to each other. The radar antenna always points to a randomly selected direction and therefore the radar's main beam may or may not hit the main beam of the Wi-Fi receiver.

5.1. Scenario TYPICAL

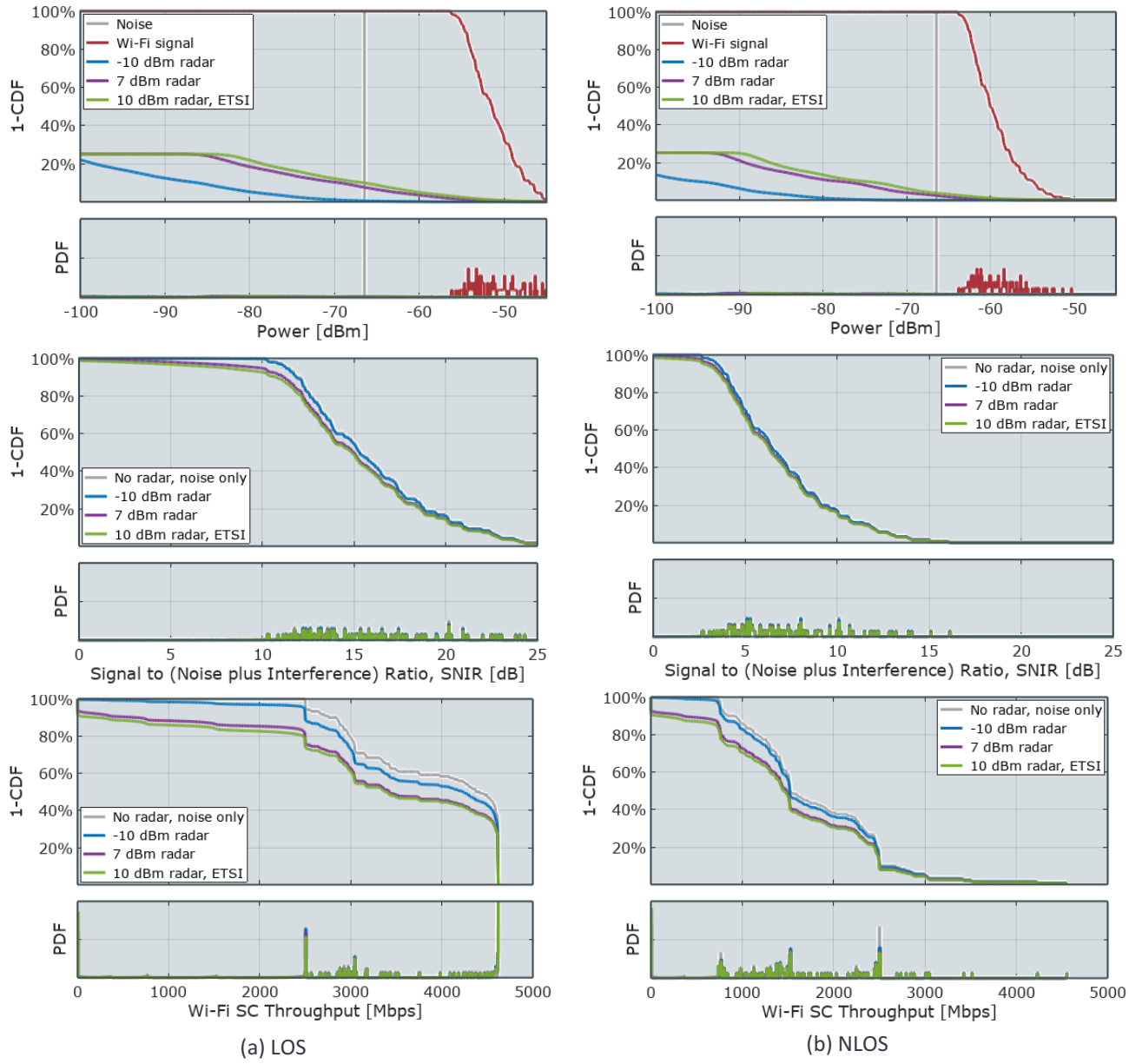

Figure 13: Simulation results for the scenario "TYPICAL" with the radar device always active.

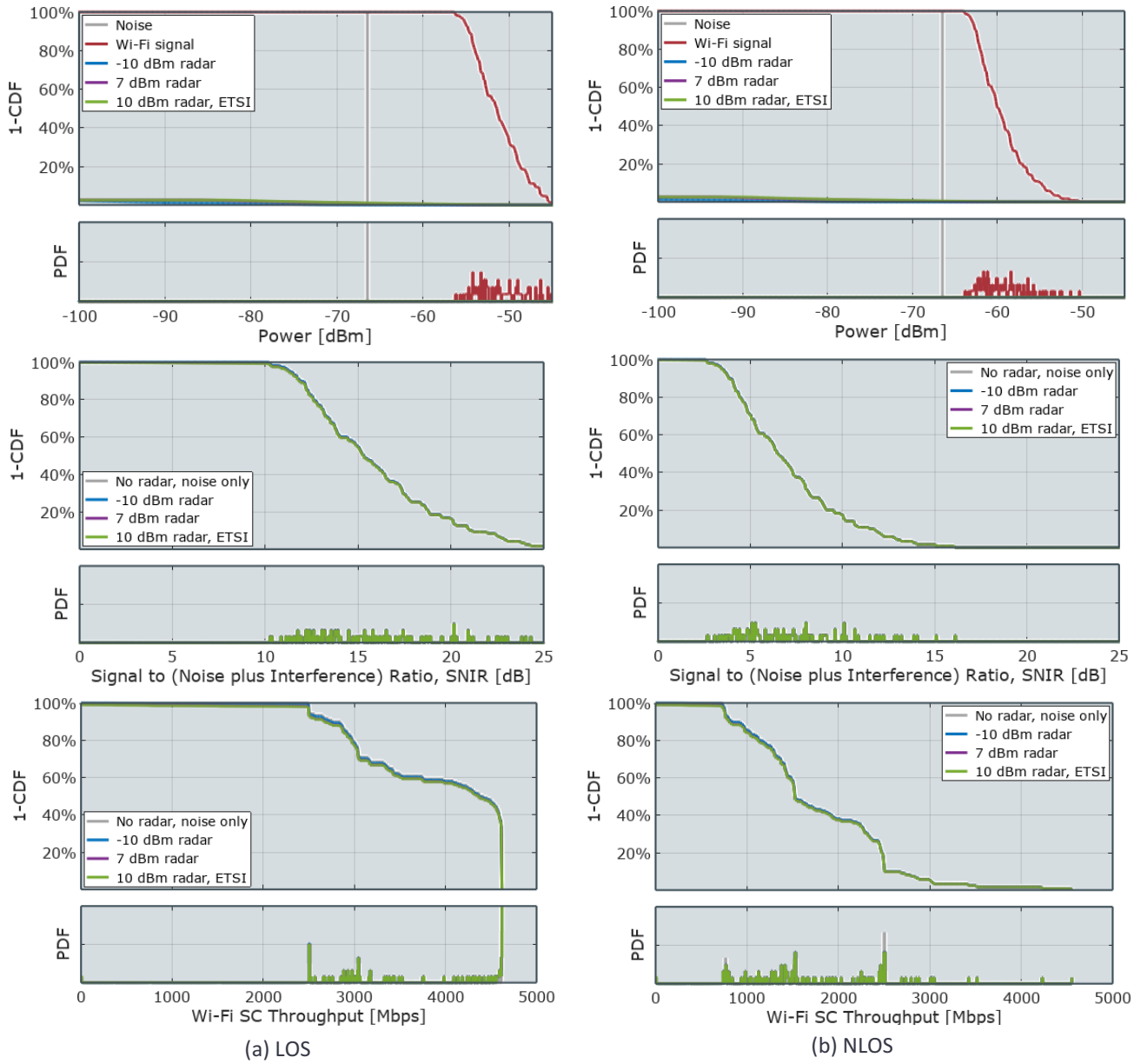

Figure 14: Simulation results for the scenario "TYPICAL" with a 10% transmit duty cycle, a conservative analysis of the expected maximum.

Figure 13 and Figure 14 show the simulation results for the scenario TYPICAL, for the LOS path loss model on the left, and the NLOS path loss model on the right. The results in Figure 14 are produced with a duty cycle of 10%. Three performance indicators are evaluated. The power of the received signals (desired Wi-Fi and interfering radar signals) at the location of the Wi-Fi station are shown in

the two figures at the top. The resulting signal to noise ratio can be found in the middle graphs, and the channel capacity or Wi-Fi throughput is shown in the bottom figures.

Multiple effects can be observed. In around 75% of the simulations, as clearly visible in the top figures, the radar operates out of band without creating any substantial interference. Together with a potential misalignment of the radar and Wi-Fi antennas (i.e., it is possible that the radar main beam would not hit the main beam of the Wi-Fi receiver), the overall resulting effect is negligible. The Wi-Fi receiver performance is not significantly compromised, regardless of the power level at which the radar is operating (-10 dBm, 7 dBm, or 10 dBm).

There are however small observable effects on Wi-Fi performance as a result of interference from the radar. With increased radar signal power, Wi-Fi is affected by up to 10% throughput reduction in the worst case.

Figure 14 shows that duty cycling mitigates the effect of the radar interference.

Overall, the radar's impact is less significant in NLOS scenarios compared to LOS. This is partially due to the fact that independent shadow fading is not taken into account in the NLOS channel models. The NLOS channel simply attenuates all signals strongly, without independent variations (radar signal and Wi-Fi signal are equally affected). Independent fading could occur in real life, but is assumed less likely here, given the short distances between the devices (in the order of meters) and the potential size of possible obstacles.

The stepwise shape of the capacity Wi-Fi throughput graphs in the two bottom figures results from the applied link adaptation.

5.2. Scenario SHORT_RANGE

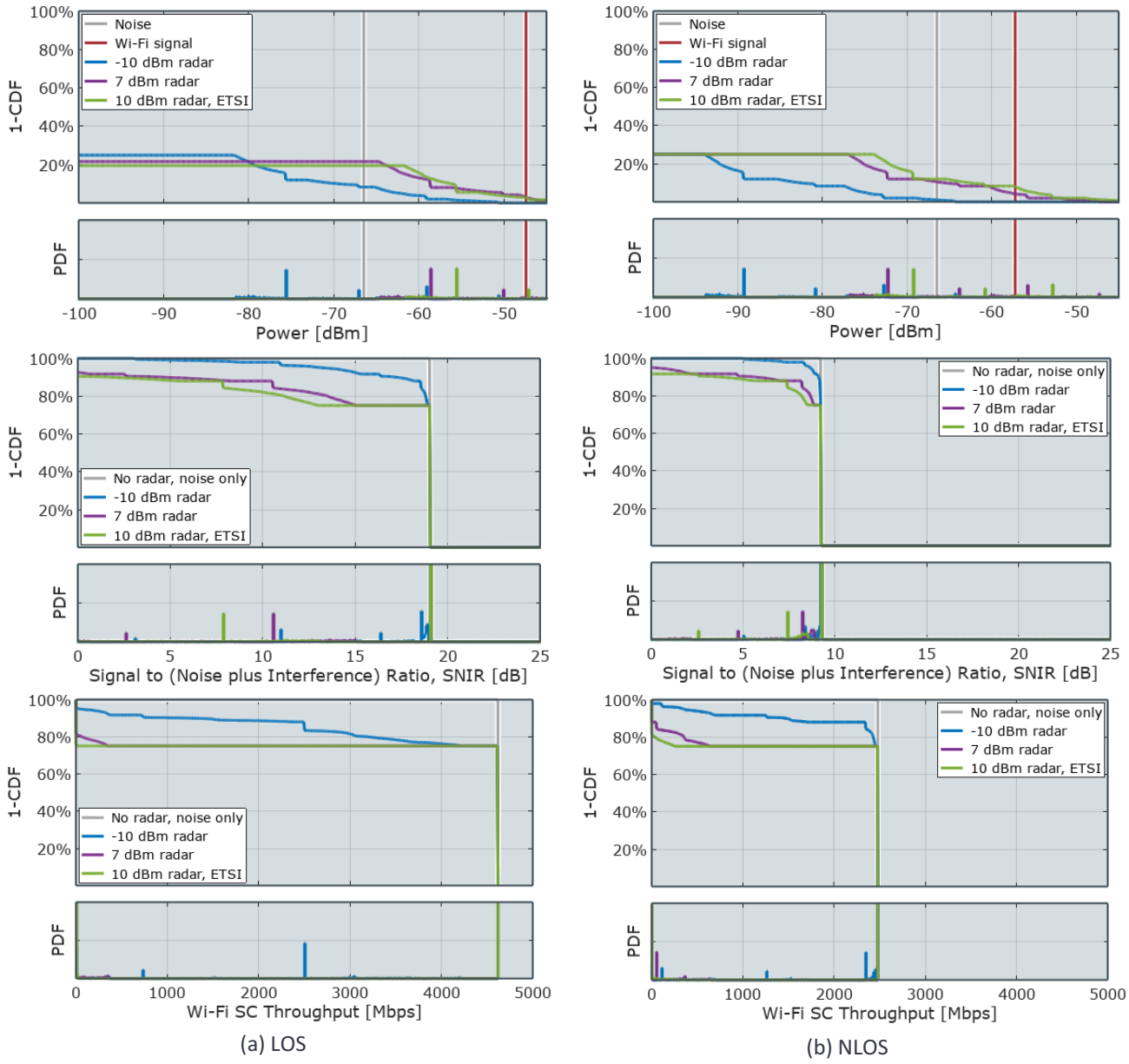

Figure 15: Simulation results for the scenario "SHORT_RANGE" with the radar device always active.

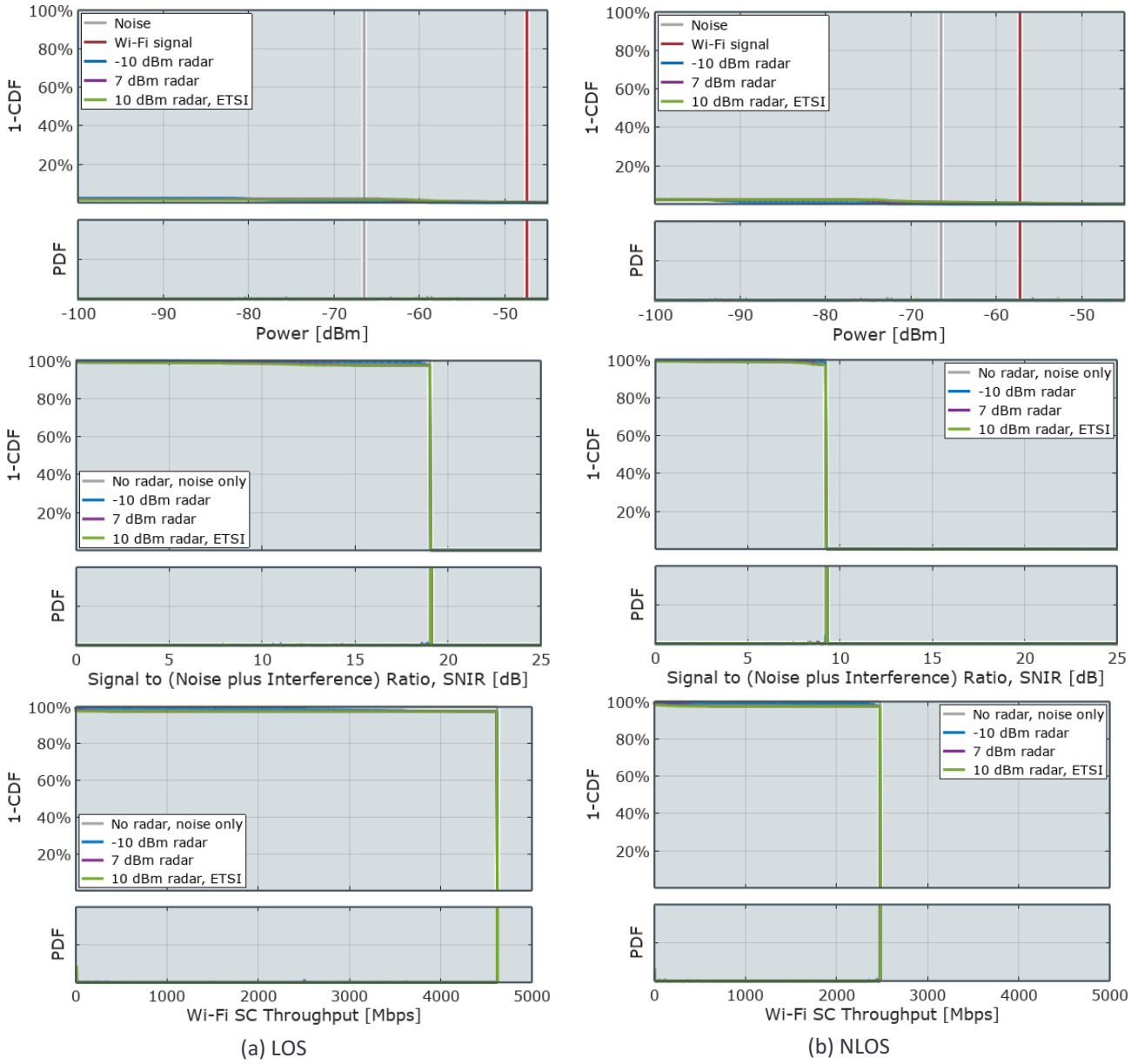

Figure 16: Simulation results for the scenario "SHORT_RANGE"with a 10% transmit duty cycle, a conservative analysis of the expected maximum.

The results of the scenario SHORT_RANGE are shown in Figure 15 for the radar device being always active, and Figure 16 for a 10% transmit duty cycle.

The effect of the out of band operation of the radar is more visible in the short range scenario. In around 75% of the experiments, the radar operates out of band without creating interference at all.

The shown Wi-Fi throughput in the bottom figures of Figure 15, however, indicates that radar devices located very closely to a receiving Wi-Fi station with the radar device always active will result in a level of interference that affects the channel capacity (if the affected Wi-Fi station is receiving from an AP further away), at around 5% to 20% of all simulations. There is, however, no significant effect on the channel capacity if the radar device operates at 10% transmit duty cycle (Figure 16).

The presented scenario is the worst case scenario, limiting the channel's availability in 10% to 20% of all simulations, if the radar device is always active. Conversely, in up to 80% to 90% of the simulations, Wi-Fi communication will not be affected at all even if the radar device is always active. And, as noted, there is no significant effect on the channel capacity when the radar device is assumed to operate at 10% transmit duty cycle.

Because of the relatively short distances between devices simulated in this scenario, similar results are obtained when changing the path loss model from LOS to NLOS (the figures for LOS, left, and NLOS, right, show the same effect).

6. Model Validation

The study in Jiang (2018) contains laboratory measurement results produced with commercially available off-the-shelf 60 GHz Wi-Fi devices. Some of the findings of the study can be used to validate the simulation model of this supplementary study.

Figure 17 shows the setup and the resulting throughput results for comparable scenarios. The Wi-Fi station is located at a distance of 15.24 meters (50 ft) away from the transmitting access point. Among other traffic configurations, downlink-only best effort (with and without interference from a co-located radar device) is used here to test if the outcome of the simulation matches the measurement.

Results are shown in Figure 17 and Table 5. For **SCENARIO 0** (no radar), the simulation model predicts slightly higher throughput outcomes for the LOS channel model (around 1300 Mbps instead of 940 Mbps). This can be explained with protocol overhead, for example the Wi-Fi listen-before-talk medium access, small packet sizes leading to control overhead, or retransmissions and sliding windows on the network layer (O'Hara and Petrick, 2005). Note that the throughput measurements were taken on the IP network layer instead of the physical layer.

Jiang et.al. (2018) defines three more scenarios that include a co-located radar for different antenna alignments and distances:

- **SCENARIO 1:** Radar directly pointing from short distance into the main beam of the Wi-Fi station's antenna
- **SCENARIO 2:** Varying short distances between radar and Wi-Fi station, and varying radar antenna directions
- **SCENARIO 3:** Radar flat on the table, at varying distances, with the radar device not necessarily pointing toward the main beam of the Wi-Fi antenna

The simulation model takes radar duty cycles and out-of-band operation into account. Therefore, the moderate effect of the radar on the Wi-Fi throughput in **SCENARIO 2** and **SCENARIO 3** are reasonably approximated. **SCENARIO 1**, however, shows the limitation of the simulation model for extreme outlier cases with heavily aligned antennas. This is not unexpected, as the antenna near fields are not modelled, and possible dynamic effects of link adaptation (changes of MCS) or protocol behaviors such as retransmissions are not taken into consideration in the simulation model.

More details about the measurement scenarios and radar system setup (e.g., duty cycle, emission power) are provided in Jiang et.al. (2018).

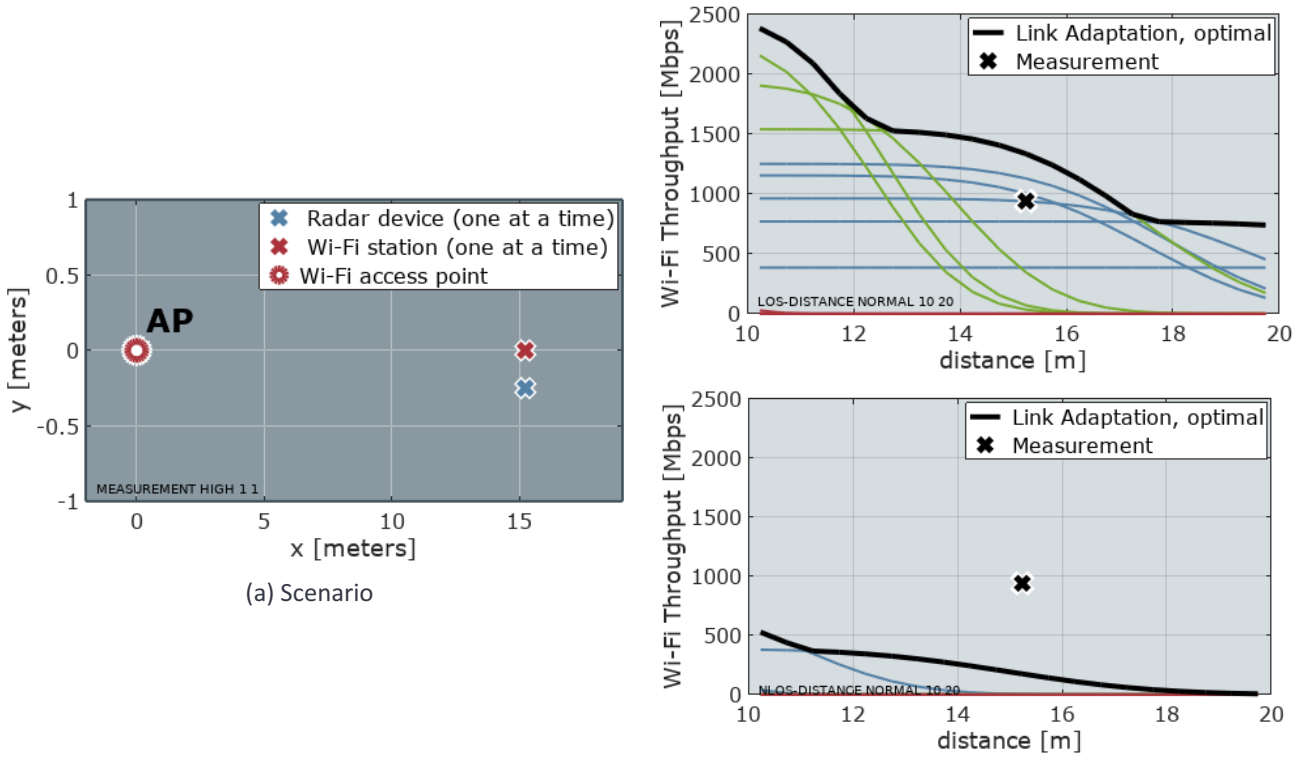

(a) Scenario

(b) Throughput results for LOS (top) and NLOS channel model (bottom)

Figure 17: Downlink measurement scenario (a, left), and throughput results for LOS and NLOS (right).

Scenario	Measured IP Layer Downlink Throughput (Jiang et.al., 2018)	Simulated Physical Layer Downlink Throughput
0	941 Mbps	1335.4 Mbps ✔
1	461 … 666 Mbps	**1322.1 Mbps ✖**
2	803 … 939 Mbps	1322.1 Mbps ✔
3	901 … 937 Mbps	1322.1 Mbps ✔

Table 5: Measurement and simulation results for downlink traffic in the scenarios described in Jiang et.al. (2018).

7. Summary and Final Remarks

This study analyzes interference effects of a radar system on 60 GHz Wi-Fi with the help of radio channel and system models. The approach is based on standard link budget models that are typically used for assessing the quality of a wireless link, or for evaluating spectral coexistence between radio systems. The Wi-Fi model presented in this study contains the IEEE 802.11ad single carrier modulation and coding schemes.

Coexistence simulation results are shown for a line-of-sight path loss channel model and a non-line-of-sight model. Both path loss models are derived from models used in literature.

This work is intended to advance discussions concerning spectral coexistence between radars and Wi-Fi at 60 GHz, while remaining simple enough to allow readers to evaluate the full model. Despite the simplicity of the simulation model, the validation in Section 6 demonstrates that the simulated throughput results are consistent with the reported outcome of laboratory tests with commercially available IEEE 802.11ad equipment.

The main findings of this supplemental study are found in Section 5. Overall, the results predict a low level of interference and confirm the results of the first study. For the given indoor scenario and with both path loss channel models, the Wi-Fi throughput is only marginally affected by interference from the radar (around 10% throughput reduction at most, if any at all). The radar duty cycling further helps to efficiently protect the operation of 60 GHz Wi-Fi. In outlier short range scenarios with co-located devices in close proximity to each other, a radar interferer can create additional interference, but only during in-band operation (around 25% of the experiments) and with the radar device always active. This effect can be greatly mitigated by radar duty cycling.

References

AXFORD (1992) **Effects of CW- and BPSK-Signal Interference on a Standard BPSK Digital Communications System**. Technical Report 1510, Naval Command, Control, and Ocean Surveillance Center RDT&E Division, Aug. 1992. www.dtic.mil/dtic/tr/fulltext/u2/a255617.pdf [accessed in 2018-04].

DIGAVI AND COVER (2001) **The worst additive noise under a covariance constraint**. IEEE Transactions on Information Theory, Vol. 47, Issue 7, Nov. 2001. ieeexplore ieee org/document/959289 [accessed in 2018-06]

IEEE 802.11AD (2014) **Enhancements for very high throughput in the 60 GHz band (adoption of IEEE Std 802.11ad-2012)**. ISO/IEC/IEEE Standard 8802-11:2012/Amd 3:2014, 2014. www.iso.org/iso/home/store/catalogue_tc/64876 [accessed in 2018-04].

IEEE 802.11 (2016) **IEEE Standard for Information technology--Telecommunications and information exchange between systems Local and metropolitan area networks--Specific requirements - Part 11: Wireless LAN Medium Access Control (MAC) and Physical Layer (PHY) Specifications**. IEEE Std 802.11-2016 (Revision of IEEE Std 802.11-2012), Dec. 14, 2016. doi:10 1109/IEEESTD 2016 7786995 [accessed in 2018-04].

JIANG AND NIJJAR AND JINDAL AND HUSTED AND WEBER (2018) **Measurement Study on Soli/11ad Coexistence.** Submission to FCC. Google LLC, May 2018.

MALTSEV AND PERAHIA AND MASLENNIKOV AND SEVASTYANOV AND KHORYAEV (2008) **60 GHz WLAN Experimental Investigations**. IEEE 802.11 Working Document 11-08/1044r0, Sep. 2008. mentor ieee org/802 11/dcn/08/11-08-1044-00-0vht-60-ghz-wlan-experimental-investigations ppt [accessed in 2018-04].

MALTSEV AND ERCEG AND PERAHIA AND HANSEN AND MASLENNIKOV AND LOMAYEV AND SEVASTYANOV AND KHORYAEV AND MOROZOV AND JACOB AND PRIEBE AND KÜRNER AND KATO AND SAWADA AND SATO AND HARADA (2010) **Channel Models for 60 GHz WLAN Systems**. IEEE 802.11 Working Document 11-09/334r8, May 2010. mentor.ieee.org/802.11/dcn/09/11-09-0334-08-00ad-channel-models-for-60-ghz-wlan-systems.doc [accessed in 2018-04].

MANGOLD (2018) **Assessing the Interference of Miniature Radar on Millimeter Wave 60 GHz Wi-Fi**. Simulation study. Lovefield Wireless GmbH, Feb-21, 2018. ecfsapi fcc gov/file/ 103071586588 94/ 2018-03-07 Soli Request for Waiver - Simulation Study pdf [accessed in 2018-04].

NITSCHE AND CORDEIRO AND FLORES AND KNIGHTLY AND PERAHIA AND WIDMER (2014) **IEEE 802.11ad: Directional 60 GHz Communication for Multi-Gigabit-per-Second Wi-Fi**. IEEE Communications Magazine, vol. 52, no. 12, pp. 132-141, Dec. 2014. doi:10.1109/MCOM.2014.6979964 [accessed in 2018-04].

O'HARA AND PETRICK (2005) **IEEE 802.11 Handbook: A Designer's Companion**. New York USA: John Wiley & Sons, Inc.. 2nd Edition. ISBN: 978-0-738-14449-8.

PERAHIA AND GONG (2011) **Gigabit wireless LANs: an overview of IEEE 802.11ac and 802.11ad**. SIGMOBILE Mob. Comput. Commun. Rev. 15, 3 (Nov. 2011), 23-33. DOI=dx.doi.org/ 10.1145/2073290.2073294 [accessed in 2018-04].

RAPPAPORT (2008) **Wireless communications: principles and practice**. Upper Saddle River, New Jersey: Prentice Hall. 2nd Edition. ISBN: 0-13-042232-0. ISBN-13: 9780130422323.

SANDERS (2012) **The Rabbit Ears Pulse-Envelope Phenomenon in Off-Fundamental Detection of Pulsed Signals**. NTIA Technical Report TR-12-487, July 2012. www.its.bldrdoc.gov/publications/ 2678.aspx [accessed in 2018-04]

SANDERS, F. AND CARROLL AND SANDERS, G. AND SOLE (2013) **Effects of Radar Interference on LTE Base Station Receiver Performance**. NTIA Technical Report TR-14-499, Dec. 2013. www ntia doc gov/report/2013/effects-radar-interference-lte-base-station-receiver-performance [accessed in 2018-04].

Appendix A: Erratum to Mangold (2018)

Page 14 states:

> "*The FMCW radar signal sweeps through a broader spectrum than one Wi-Fi channel and creates interference only at a fraction of time. However, the sweep time is short. To sweep through one Wi-Fi channel takes less time than the duration of one Wi-Fi OFDM symbol duration (~242 us, see Table 1). Hence, a Wi-Fi data packet transmission is usually affected by multiple repeated sweeps. For this reason, the out-of-channel time is ignored and a continuous interference (worst case assumption) is assumed.*" [Mangold, 2018]

This statement is not correct. One Wi-Fi OFDM symbol duration is around 242 nanoseconds, and not 242 microseconds as stated in the quoted text. It is therefore not possible that multiple repeated sweeps from the same radar device will affect one OFDM symbol. The assumption that there will always be interference on the frequency channel is therefore too pessimistic, even if the radar device were always to be active. Instead, in only 1 out of 4 experiments (around 25% probability), the Wi-Fi channel under investigation will be affected at all. This is taken into account in the supplemental study.

Appendix B: Implementation Details

```
function samples_W = estimate_interference(x_radars, y_radars, x_WiFi, y_WiFi, P_Tx_radar_W, Gt, Gr, isNlos, ANTENNACONFIG)

 I = [];
 radar_positions = [];
 samples_W = [];

 for wificnt = 1:size(x_WiFi,2)
  samples01_W = []; % this construct is needed to speed up the simulation

  for radarcnt = 1:size(x_radars,2)
  switch ANTENNACONFIG
    case "HIGH"
      one_P_Tx_radar_W = P_Tx_radar_W;
      one_Gr = Gr;
    case "NORMAL"
      if rand < .66666667 % Given the antenna pattern of the radar device (-60..+60 degree), in 66%,
                          % P_Tx_radar is reduced. Impact will be minimal.
        one_P_Tx_radar_W = P_Tx_radar_W .* ( 10.^((Gt_reverse_Radar_dBi-Gt_Radar_dBi)./10));
      else
        one_P_Tx_radar_W = P_Tx_radar_W; % this is the direct hit case, maximum impact on Wi-Fi.
      end
      if rand < .75 % in 75%, Gr_WiFi is reduced to 0dBm:
        one_Gr = 0; % this is the Wi-Fi reverse case with minimal impact.
      else
        one_Gr = Gr; % this is the direct hit case on the Wi-Fi receiver, with maximum impact on Wi-Fi
      end

      if rand > FreqCollisionProb % 7000MHz/1760MHz ... Gr_WiFi is reduced to -100dBm
        one_Gr = -100; % this is the OUT OF BAND OPERATION.
         end
    case "LOW"
      one_P_Tx_radar_W = P_Tx_radar_W .* ( 10.^((Gt_reverse_Radar_dBi-Gt_Radar_dBi)./10));
      one_Gr = 0;
    otherwise
      error ("unknown config for ANTENNACONFIG");
    endswitch

    [rx_W] = rxpower(one_P_Tx_radar_W, x_radars(radarcnt), y_radars(radarcnt), x_WiFi(wificnt), ...
              y_WiFi(wificnt),Gt,one_Gr, isNlos);
    samples01_W = [samples01_W rx_W'];

  end

  samples_W = [samples_W samples01_W];

endfunction

```

Code 1: Interference estimation.

```
function [C_bps100_max C_bps2000_max C_bps100 C_bps2000 Eav2N0 BER PER100 PER2000] =
    capacity_SC(P_Rx_W,I_W,N_W)
          for mcs_cnt = 1:size(ScSensitivity_W,2)
          outofSensitivityRange(1,:,mcs_cnt) = P_Rx_W < ScSensitivity_W(mcs_cnt);
          endfor
          %% ---- Continues Wave interference instead of Gaussian noise
          I_W = I_W .* 50;
          if ~isempty (I_W)
                                Eav2N0 = P_Rx_W ./ (I_W + N_W);
          else                  Eav2N0 = P_Rx_W ./ N_W;
          endif
          ScCodingGain    (1,1,:) = 10.^ (ScCodingGain_dB(ScModulationIndex2 ...
                                +1:size(ScModulationIndexM,2))/10);
          ScCodingGainBPSK(1,1,:) = 10.^ (ScCodingGain_dB(1:ScModulationIndex2)/10);
          %% ---- M>2 (QPSK, 16QAM)
          ScModulationIndexM_QAM = ScModulationIndexM(ScModulationIndex2+1: ...
           size(ScModulationIndexM,2)); % take out all BPSK, M=2
          ScModIndex (1,1,:) = ScModulationIndexM_QAM;
          P_sqrtM = 2 .* (1 - 1 ./ sqrt(ScModIndex)) .* ...
          Q(sqrt(3 ./ (ScModIndex-1) .* Eav2N0 .* ScCodingGain)); %Symbol Error Rate P_sqrt(M)
          P_M = 1 - (1-P_sqrtM).^2; %Symbol Error Prob (QAM): P_M = 1-(1-P_sqrt(M))^2
          BER_QAM = P_M ./ log2(ScModIndex); % Bit Error Ratio BER(M)=1/log2(M) * P_M

          %% ---- M=2 (BPSK)
          BER_BPSK = Q(sqrt(2 .* Eav2N0 .* ScCodingGainBPSK));
        % Bit Error Ratio (BER)(BPSK): BER(2) - directly from Eb/N0

          %% ---- putting all modulations together into BER:
          BER (:,:,1:ScModulationIndex2) = BER_BPSK;
          BER (:,:,ScModulationIndex2+1:ScModulationIndex2+size(ScModulationIndexM_QAM,2)) = BER_QAM;
          %% ---- when the device is out of coverage range, we set BER to 1
          BER = max(BER,outofSensitivityRange);
          %% --- Packet Error Ratio PER n
          CodeWordSize_bit = [672 2000]; % code word length, 100 byte = 800 bit. 672 is default
          PER100  = 1 - (1-[BER]).^CodeWordSize_bit(1);
          PER2000 = 1 - (1-[BER]).^CodeWordSize_bit(2);
          for cnt_a = 1:size(PER100,1)
                    for cnt_b = 1:size(PER100,2)
                                codes(cnt_a,cnt_b,1:size(ScCodingOverhead,2)) = ScCodingOverhead;
                                rate(cnt_a,cnt_b,1:size(ScMaxDatarate_bps,2)) = ScMaxDatarate_bps;
          end     end
          %% --- Resulting Link Throughput in b/s
          C_bps100  = (codes) .* (1-PER100)  .* rate;
          C_bps2000 = (codes) .* (1-PER2000) .* rate;
          C_bps100  = C_bps100 * ScGolayLoss;
          C_bps2000 = C_bps2000 * ScGolayLoss;
          C_bps100_max = max(C_bps100,[],3);     %% link adaptation
          C_bps2000_max = max(C_bps2000,[],3);
endfunction
```

Code 2: Single Carrier MCS Model

```
function [Rx_W] = rxpower(Tx_W,x_Tx,y_Tx,x_Rx,y_Rx,Gt,Gr, isNlos)
        distance_m = sqrt((x_Tx-x_Rx) .^2 + (y_Tx-y_Rx).^2);
        distance_m = max(distance_m,.5);  # assume distance>d0

        if isNlos AA = 44.7; nn = 1.5;
        else AA = 32.5; nn = 2;  end

        ploss_dB = AA + 20 .* log10(60.48) + 10 .* nn .* log10(distance_m); % from 802.11ad
        Tx_dBW = 10 * log10 (Tx_W);
        Rx_dBW = Tx_dBW - ploss_dB + Gt + Gr;
        Rx_W = 10 .^ (Rx_dBW ./ 10);
endfunction
```

Code 3: Path loss model.

ATTACHMENT B

Measurement Study on Soli/802.11ad Coexistence

Qi Jiang, Raj Nijjar, Nihar Jindal, Paul Husted, Dave Weber
Google LLC
June 2018

Summary

1. Measurements with commercially available 802.11ad equipment confirm that Soli technology does not create interference to most 802.11ad links.

2. For a measurable effect to be seen, Soli must be positioned directly between the 802.11ad client and access point (AP), with the Soli antenna pointing directly into one of the 802.11ad antennas. This is an unlikely placement because Soli gesture-sensing technology is intended to face the user and rarely will be active when not in a user-facing position.

3. A comparison of the worst-case interference due to Soli being in close proximity relative to another 802.11ad client in close proximity shows that Soli creates less degradation to 802.11ad networks than 802.11ad networks cause to themselves.

Introduction

Google's Project Soli gesture-sensing technology and IEEE 802.11ad devices both operate within the 60 GHz spectrum band. Some parties have raised concerns about the specific scenario when Soli and 802.11ad systems operate within close proximity to one another.

This study provides actual laboratory measurement data focusing on the scenario in which a device that includes Soli technology is present at various locations very close to the 802.11ad link, and characterizes the potential impact from Soli technology on 802.11ad devices and/or link performance. The results of bandwidth sharing between a Soli device and an 802.11ad link is then compared to sharing between one 802.11ad network and another 802.11ad network on the same channel.

This study is intended to supplement and complement two simulation-based studies created by Lovefield Wireless, which have been filed at the Federal Communications Commission (FCC) in *Request by Google LLC for Waiver of Section 15.255(c)(3) of the Commission's Rules*, ET Docket No. 18-70.

The study is organized into three sections:

1. Analyzing the impact of interference from Soli technology on an 802.11ad link, using commercially available 802.11ad devices
2. Examining the impact of adding an 802.11ad link on the same channel as an existing 802.11ad link, as a point of comparison, again using commercial available 802.11ad devices
3. Conclusions

Impact of Soli technology on 802.11ad links

In this section, Soli technology is presented as the interferer to the existing 802.11ad link at a number of different locations with respect to the 802.11ad link. To characterize the link performance, active iPerf TCP traffic within the 802.11ad link is run with and without the Soli technology transmitting.

Test Setup

The test was conducted in an indoor office environment without people present in the vicinity of the test setup. Test equipment was comprised of:

1. 1x Netgear Nighthawk X10 R9000 802.11ad AP
2. 1x Acer laptop (N16C5) with built-in 802.11ad capability
3. 1x Infineon Soli reference board (BGT60TR24C application board)

A desktop server was connected via 1Gbps Ethernet to the Netgear AP, which ran the iPerf server. A MacBook Pro laptop (not pictured below) was used to control the Soli board.

A diagram of the test setup is below:

For the purposes of this study, “uplink test” refers to a transfer of data from the 802.11ad client laptop to the 802.11ad AP, and “downlink test” refers to a transfer of data from the 802.11ad AP to the 802.11ad client laptop. In this test, the max WiGig throughput may be limited by the 1Gbps Ethernet connection that was used, which is commonly employed in residential and commercial office deployments. Other Ethernet connections (e.g., 10GigE) that are less commonly used could yield different results. Note that our goal is not to evaluate the 11ad maximum throughput but to compare the relative effect of channel sharing in a common setup. The 1Gbps Ethernet connection is used consistently for both Soli interference and 802.11ad interference testing. Furthermore, experimentation as well as link budget analysis based upon the 50ft distance between 11ad devices revealed that the limitation due to the 1 Gbps Ethernet connection was not significant.

An Infineon reference design was used as the Soli device. This device was operated in the following condition, which corresponds to the currently expected duty cycle for the Soli gesture sensing technology when it is active during a triggering event:

- TX conducted power: +7dBm
- TX max antenna gain: +6dBi
- Frequency of chirp: 57.5 - 63.5GHz
- Duration of chirp: 37us
- Chirp repetition rate: 1400Hz

The duty cycle studied here is based on actual expected device characteristics, and is lower than the duty cycle Lovefield Wireless conservatively assumed in its simulations. This duty cycle is also the expected maximum when the Soli technology detects a gesture; the steady state duty cycle (when no gesture is detected) is expected to be much lower.

The TX output power of the Infineon BGT60TR24C reference design represents the maximum power located on the market for the Soli application as of the date of this study.

Soli Placement Relative to 802.11ad Antenna

The antenna in the Acer 802.11ad laptop is located at the upper left corner of the screen, as shown in the following figure.

The Soli technology was positioned in various configurations with respect to the 802.11ad antenna, and at various distances for each configuration. The different locations are shown in the figures below. As noted above, the purpose of this study is to examine close-range interference. Accordingly, distances between one inch and one foot were tested. In order to test

performance in worst-case (albeit unlikely) scenarios, testing was first conducted in configurations purposely chosen to maximize interference to the 802.11ad link, after which configurations more realistic for consumer use were tested.

Configuration 1: Soli technology directly pointed at the 802.11ad antenna

a. Soli technology one inch away from the 802.11ad antenna. This position was chosen through experimentation as the point where the maximum throughput degradation occurred when Soli was active.

1-a

1-a

b. Soli technology five inches away from the 802.11ad antenna

1-b

c. Soli technology one foot away from the 802.11ad antenna

1-c

Configuration 2: Soli technology pointed at the side of the 802.11ad antenna

a. Soli technology pointed at the near side of the 802.11ad antenna, one inch away

2-a

b. Soli technology pointed at the far side of the 802.11ad antenna, one inch away

2-b

Configuration 3: Soli technology placed flat on the table with beam pointing directly upward, to mimic a user placing a device on a table

a. Soli technology five inches away from the screen in front of the laptop

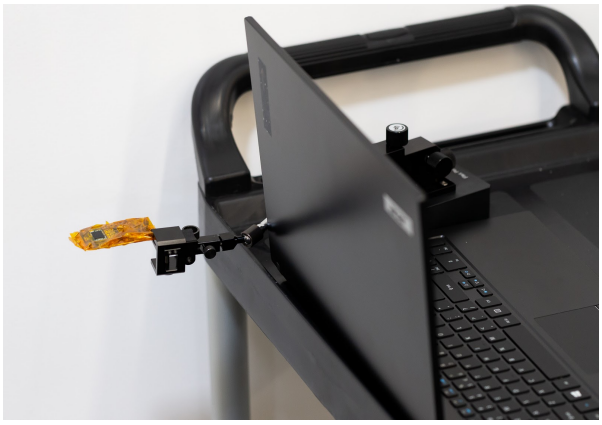

3-a

b. Soli technology one inch away from the screen in front of the laptop

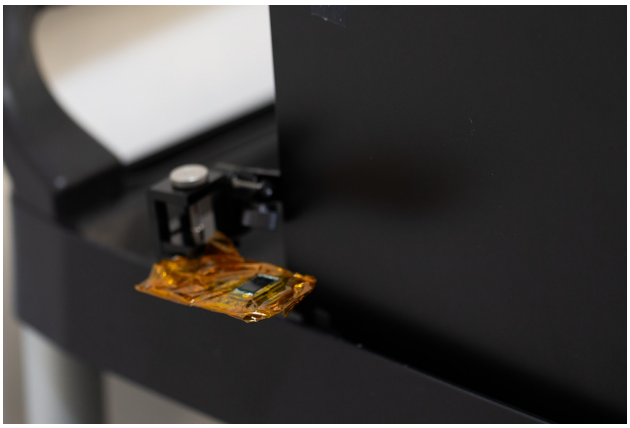

3-b

c. Soli technology placed at the near side of the 802.11ad antenna, one inch away

3-c

d. Soli technology placed one inch from the screen at the keyboard

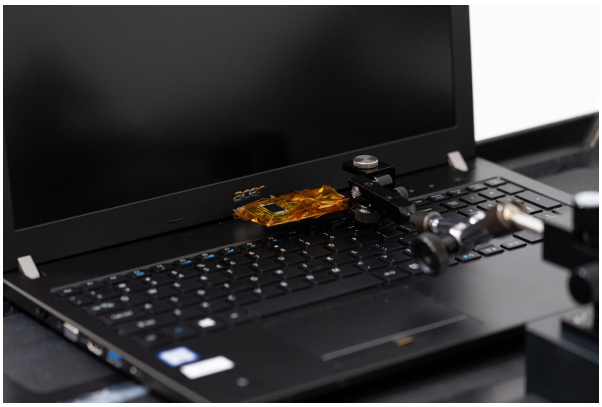

3-d

e. Soli technology placed at the end of the keyboard, one inch away

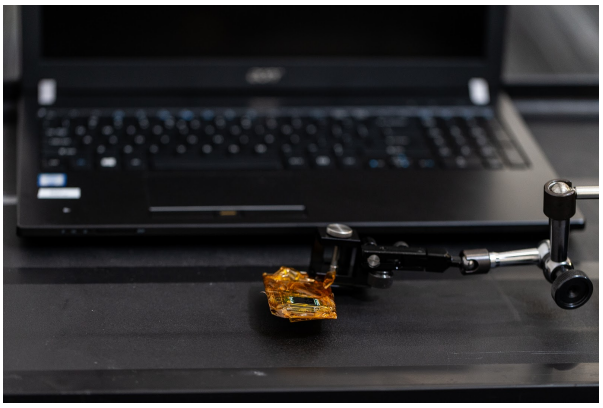

3-e

f. Soli technology placed at the far side of the 802.11ad antenna, one inch away

3-f

Test Procedure

At the locations above, the 802.11ad link performance was measured both with the Soli technology transmitting and with Soli turned off. The test procedure was as follows:

a. Measure both uplink and downlink throughput for a clean 802.11ad link without the Soli technology.
b. Move the Soli technology to the position described above.

c. Measure both uplink and downlink throughput in sequence with the Soli technology turned off.
d. Measure both uplink and downlink throughput in sequence with the Soli technology turned on.
e. Move the Soli technology to the next position and repeat steps b to d.

Results

In this test, the 802.11ad link was 50 feet long and operated on channel 2, which spans 59.40 - 61.56 GHz and thus falls inside the Soli chirp frequencies of 57.5 - 63.5 GHz. Both uplink and downlink iPerf traffic were measured. The test results are presented in the table below. (Position 0 is the 11ad link only without the Soli technology, i.e., (a) in the above Test Procedure description; throughput is displayed in Mbps).

Traffic	**Soli Status**	**Ref**	**Positions (Soli pointing directly at victim antenna)**					
		0	**1-a**	**1-b**	**1-c**	**2-a**	**2-b**	
Uplink	**ON**	937	764	837	845	862	939	
	OFF		937	934	940	935	937	
Downlink	**ON**	941	461	563	666	803	939	
	OFF		940	935	937	940	938	
Traffic	**Soli Status**	**Positions (likely positions with Soli next to device)**						
		3-a	**3-b**	**3-c**	**3-d**	**3-e**	**3-f**	
Uplink	**ON**	888	891	929	914	929	935	
	OFF	933	937	938	935	937	935	
Downlink	**ON**	901	920	935	935	937	934	
	OFF	942	939	938	937	937	938	

Analysis

The impact of the Soli technology on the 802.11ad link depends on where the Soli is positioned. Unless the Soli transmitter is pointing directly into the 802.11ad antenna and is extremely close to the 11ad antenna, as in position 1-a, b, and c, the presence of the physical Soli device does not substantially degrade the 802.11ad link. For Position 1-a, when the Soli device is placed one inch away from the front of the 802.11ad antenna, 50% degradation of throughput for downlink traffic is observed due to the Soli transmitter interference. When the Soli device is moved away from the 802.11ad antenna, the throughput degradation observed is about 40% at a distance of five inches away and 30% at one foot away. For uplink traffic where the laptop is transmitting, the impact is much lower than for the downlink.

In the much more likely configuration 3 (Soli lying flat on a table and pointing straight up), Soli has virtually no effect on the 11ad throughput.[1]

Impact of an additional 802.11ad link to an existing 802.11ad link

In this section, the Soli technology was removed from the above test setup, and replaced with a second 802.11ad radio connected to a second 802.11ad AP to measure the impact of adding a new 802.11ad link (Link-B) to the environment with the existing 802.11ad link (Link-A). Both links used identical laptop clients and 802.11ad APs, and both links used 802.11ad channel 2. Both links were at good signal condition, as in the above tests measuring the impact of Soli technology on the 802.11ad link. Laptop B was placed so that its beamforming algorithms could be in the general direction of Laptop A, allowing for a comparison to the interference generated by Soli technology.

Test Setup

Here is the general diagram of this measurement.

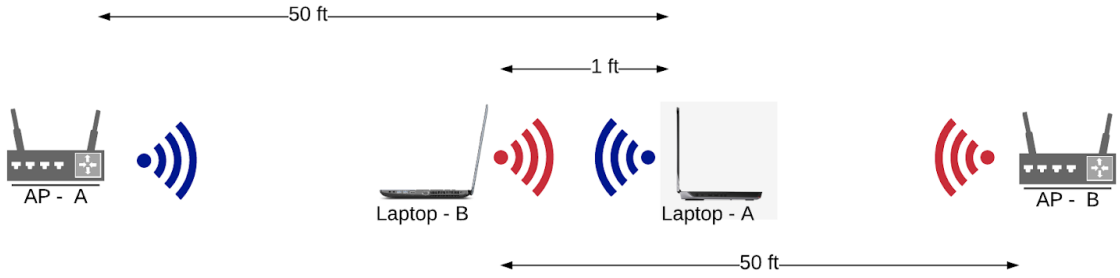

During the measurement, Laptop-B was placed in two positions with respect to Laptop-A as shown below.

[1] Potential interference from Project Soli technology with 802.15.3e as a near-proximity communications standard is even less likely to arise than for 802.11ad, because the intended range for 802.15.3e is 10 cm or less, much shorter than for 802.11ad. IEEE Standards Assoc., *IEEE Standard for High Data Rate Wireless Multi-Media Networks Amendment 1: High-Rate Close Proximity Point-to-Point Communications*, § 4.1a (June 2017), *available at* https://ieeexplore.ieee.org/document/7942281/. This study confirms the general principle that at 60 GHz interference occurs mainly when the interfering technology is directly between the communications link, with the interfering antenna pointed directly at the victim antenna. Because this is less likely to occur when the communications link operates at 10 cm, Project Soli's potential interference with an 802.15.3e link is practically much lower.

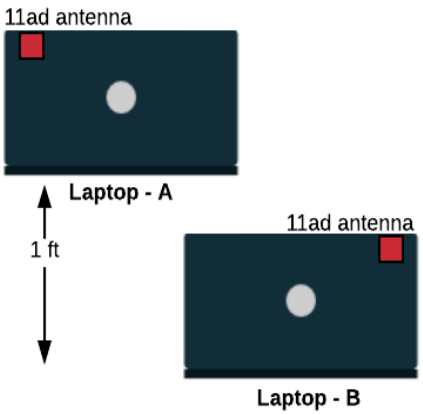

Position #1

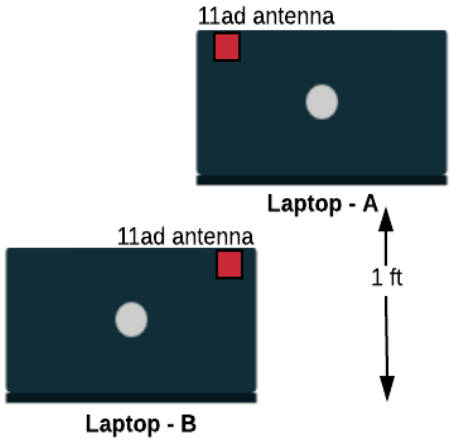

Position #2

The figures in Appendix B illustrate the positions between two 802.11ad laptops during tests. For Position #1, both laptops have clear line of sight (LoS) from their respective antennas to their respective APs; for Position #2, the 802.11ad antenna of each laptop is blocked by the other laptop, similar to the position in which the Soli technology was pointed directly toward the 802.11ad antenna for position #1 in the preceding section.

Distance between two 11ad laptops

Test Procedure

The same iPerf TCP traffic method was used to characterize the impact on link performance. The test procedures were:

a. The two laptops were moved to Position #1.
b. The individual uplink and downlink throughput for each link with the other link not running was measured.
c. The following combination of traffic tests were executed:
    i. Link-A downlink and Link-B downlink
    ii. Link-A downlink and Link-B uplink
    iii. Link-A uplink and Link-B downlink
    iv. Link-A uplink and Link-B uplink
d. The laptops were moved to Position #2 and steps b and c were repeated.

As a baseline reference, the individual throughput in Mbps without the other 802.11ad link running is listed below.

Position	Traffic	Link-A	Link-B
1	**Downlink**	913	903
	Uplink	936.5	935.5
2	**Downlink**	937	896.5
	Uplink	936	916.5

The simultaneous traffic combination results are shown below.

Position	Traffic	A-DL + B-DL	A-DL + B-UL	A-UL + B-DL	A-UL + B-UL
1	**Link-A**	741	559	672	624
	Link-B	288	430	384	546
	Average	**515**	**495**	**528**	**585**
2	**Link-A**	430	213	610	502
	Link-B	264	540	181	483
	Average	**347**	**377**	**396**	**493**

The case in which one link is on uplink and the other is on downlink (especially for Position #2) is similar to where the Soli technology is transmitting to the 802.11ad antenna when the 802.11ad laptop is running downlink traffic.

Notably for position 2, when one link is in uplink and one link is in downlink, the downlink is impaired more than the uplink. This may be because listen before talk is not reliable in beamformed systems[2] in the configuration of position 2, where the AP is in the back lobe of the interfering client of the other network, and therefore may not receive signals above the clear channel assessment level.

Conclusions

The tests described above yield two main conclusions:

Soli technology does not create significant interference to most 802.11ad links.
Based on the configurations studied here, for Soli technology to negatively impact 802.11ad links, *all of the following* must be true:

1. Soli technology must be positioned directly between the AP and client.

[2] *Deafness: A MAC Problem in Ad Hoc Networks when using Directional Antennas,* Proc. ICNP, Oct. 2004.

    - Scenario 2 shows that if Soli technology is pointing at the 802.11ad antenna but not between the client and the AP, there is no noticeable interference.
2. Soli technology must be directly facing the 802.11ad receiver with an unobstructed path.
    - Scenario 3 shows no impact if Soli technology is placed in a position facing the antenna at 90 degrees.
3. Soli technology must have a short distance, unobstructed path to the 802.11ad antenna.
    - This scenario is very unlikely because use cases of Soli technology are based on interaction with a user directly above the Soli sensor.

As noted, Requirement 3 (short distance with unobstructed path) is itself unlikely to occur. The simultaneous occurrence of short distance and unobstructed path together with placement directly between the 802.11ad AP and client, where the Soli device is directly facing the 802.11ad receiver, is even more unlikely.

Soli technology impacts 802.11ad significantly less than adding another 802.11ad link.[3]

- Even with Soli technology positioned just one inch away from the 802.11ad device, average (UL+DL)/2 802.11ad throughput was 612.5 Mbps.
- This was greater than the average per-link performance of any scenario of uplink or downlink for either link in either position 10 inches away from each other, with two 802.11ad links in use simultaneously.
    - These results ranged from 347 to 585 Mbps in the tests described above.
    - Total 802.11ad throughput of both links may be higher, but this study focuses on the impact to a single user of adding a new radio to a given environment.

[3] Duty cycle is different between the two technologies. In this comparison both technologies were tested at their maximum duty cycle.

ATTACHMENT C

Compatibility between Earth Exploration-Satellite Service Sensors and Airborne Use of Project Soli Devices at 57.5 to 63.5 GHz

Andrew W. Clegg, PhD
Google LLC
June 2018

1. Background

The frequency range used by Project Soli, 57.5 to 63.5 GHz, partially overlaps the 57 to 59.3 GHz band allocated for the earth exploration-satellite (passive) service (EESS). EESS uses passive sensors on orbiting satellites for various remote sensing purposes, including weather forecasting and military applications.[1] Atmospheric attenuation from the ground to space is sufficiently large that there is no concern over interference to the satellites caused by ground-based use of devices that incorporate Soli technology (Soli devices). However, the attenuation to space from Soli devices at high altitudes, such as those on board commercial aircraft at cruising altitude, raises a potential concern. The National Academy of Sciences' Committee on Radio Frequencies (CORF) performed a basic calculation in its comments suggesting that interference generated by airborne use of Soli devices could approach the harmful interference threshold of spaceborne sensors.[2] However, a more detailed analysis that considers bandwidth overlap, transmit duty cycle, aircraft design, transmitter/receiver geometry, and atmospheric attenuation shows that Soli devices operating at the power levels requested in Google's petition for waiver in ET Docket No. 18-70 will not cause interference to EESS sensors.

2. Interference Considerations into Known EESS Sensors

Significant considerations related to predicting interference from Soli devices into known EESS sensors include:

1. Effective Isotropic Radiated Power (EIRP) of Soli devices in the frequency range of channels used by EESS sensors
2. Relative geometry between Soli devices and the EESS sensors
3. Atmospheric attenuation between Soli devices and the EESS sensors
4. Maximum interference power, based on the combination of considerations (1) and (3)
5. Number of Soli devices that collectively contribute to interference
6. Antenna gain of the EESS sensors
7. Protection criterion for the EESS sensors
8. Interference margin

---

[1] C.f. Comments of Nat'l Acad. of Scis.' Comm. on Radio Frequencies in ET Docket No. 18-70 at 1 (filed Apr. 20, 2018) (CORF Comments).
[2] *Id.* at 6-8.

Each factor is discussed below. Sections 2 and 3 apply the specific EESS sensor characteristics that are listed in Appendix A, and the characteristics of Soli technology that are listed in Appendix B. Section 4 more broadly discusses Soli's compatibility with EESS. Section 5 addresses additional factors that are not incorporated in this analysis.

2.1 EIRP of Soli Devices in the Frequency Range Received by EESS Sensor Channels

Soli devices sweep over a 6 GHz frequency range from 57.5 to 63.5 GHz. Known EESS sensors that have channels within this range are:

- Advanced Microwave Sounding Unit-A (AMSU-A)
- Advanced Technology Microwave Sounder (ATMS)
- Special Sensor Microwave Imager/Sounder (SSMIS)

Figure 1 shows the distribution of the sensors' channels with respect to the Soli sweep range and the EESS (passive) allocation.

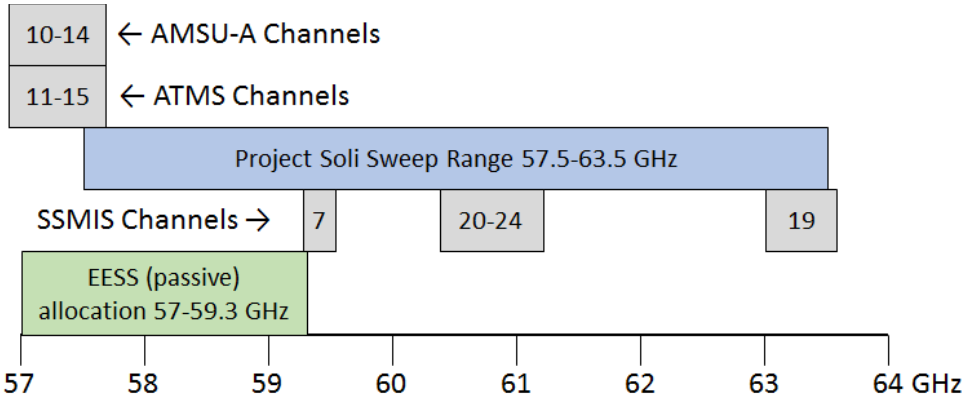

Figure 1: Frequency of AMSU-A, ATMS, and SSMIS sensor channels with respect to the Soli sweep range and the EESS (passive) allocation.

Soli devices sweep across their entire 6 GHz range at a rate much faster than the integration times of the EESS sensors. Therefore, the effective EIRP of a Soli device within a given sensor channel must take into account the fraction of time the chirped signal is within the channel's frequency range. Because Soli uses a linear frequency modulation (FM) chirp, that fraction of time is simply the ratio of sensor channel bandwidth contained within the Soli sweep range to the total Soli sweep range, which (in dB units) is $10\log_{10}(\text{OBW}/6\text{ GHz})$, where OBW (the overlap bandwidth) is the overlap of the sensor channel with the Soli device's sweep range. For example, if a sensor channel overlaps with 100 MHz of the Soli device's sweep range, then a Soli sweep spends 100 MHz/6000 MHz = 1.67% of its time within that channel. Because the sweep is much faster than the sensors' integration times, the Soli device EIRP within that channel is effectively reduced by a factor of $10\log_{10}(100\text{ MHz}/6000\text{ MHz})$ = -17.8 dB. The

overlap bandwidth equals the sensor channel bandwidth if the channel is entirely contained within the Soli device's sweep range, otherwise, the overlap bandwidth is that amount of the channel bandwidth that falls within the Soli device's sweep range.

Further, Soli devices do not emit constantly. Instead, during normal operation and on a time scale that is short compared to the sensor integration times, a burst of sweeps is emitted, followed by a silent period before the next burst of sweeps is emitted. The maximum fraction of time that the device is transmitting (i.e., the duty cycle) of a Soli device is approximately 10% over the integration period of the sensors. Therefore, the effective EIRP of a Soli device within a sensor channel is further reduced by a duty cycle correction factor of 10 dB.

The net EIRP of a Soli device within a sensor channel is equal to the Soli EIRP (13 dBm), with both the overlap correction factor and the duty cycle correction factor applied. For the example of the 100 MHz channel falling entirely within the Soli device's sweep range, the net EIRP of the Soli device is 13 dBm - 17.8 dB - 10 dB = -14.8 dBm.

Google requests a waiver from the Commission to operate Soli devices up to a maximum EIRP of 20 dBm, which is harmonized with the European standards for similar devices in the 60 GHz band. However, Soli hardware components currently available have a maximum measured EIRP of not more than 13 dBm. For the purpose of realistic assessment, this analysis primarily uses the measured EIRP. To augment the information available for the Commission's review, however, this analysis also considers the interference margin when Soli devices operate at the requested maximum EIRP of 20 dBm. Operation of Soli devices is shown to easily meet the interference criterion for the EESS sensors, even at 20 dBm EIRP.

2.2 Geometry between Soli Device and Sensor Antenna

Concern has been raised about the impact on EESS satellite sensors caused by Soli transmissions in airplanes at high altitudes. Therefore, the amount of radiation escaping the airplane is a consideration. The issue is addressed in ITU-R Report M.2283-0, which concerns radiation from Wireless Avionics Intra-Communications (WAIC) systems installed in commercial passenger aircraft. The ITU-R Report concludes that "[t]he dominant leakage mechanism for WAIC signals originating from within the fuselage is through the cabin windows."[3] Aircraft windows, which measure approximately 10 inches wide by 14 inches tall and consist of multiple layers of acrylic, are effectively rectangular apertures through which signals are emitted out of the side of the plane. Further, millimeter wave signals such as those emitted by Soli devices have very small levels of diffraction. Thus, it can be reasonably assumed that signals emanating through these apertures are effectively collimated into a beam that is formed by the projection of the signal source (i.e., a Soli device) through the rectangular aperture, broadside to the plane,

[3] Int'l Telecomm. Union, *Technical Characteristics and Spectrum Requirements of Wireless Avionics Intra-Communications Systems to Support Their Safe Operation*, ITU-R Report M.2283-0 at 21 (Dec. 2013), *available at* https://www.itu.int/dms_pub/itu-r/opb/rep/R-REP-M.2283https://www.itu.int/dms_pub/itu-r/opb/rep/R-REP-M.2283-2013-PDF-E.pdf-2013-PDF-E.pdf.

with no significant diffraction of the radiated emissions outside of that collimated beam. It is then a straightforward matter to simulate the beam emanating from the plane, as a function of the location of the Soli device inside the plane with respect to the nearest window from which the signal emanates.

For this simulation, the attenuation of the window is taken to be 0 dB. This is a highly conservative assumption. In fact, based on the construction of the windows, combined with reflection and material absorption losses of the acrylic material at 60 GHz, the attenuation at normal incidence to the window is predicted to be approximately 11.6 dB, and attenuation at the maximum oblique incidence of 79 deg is 25.8 dB.[4] Total internal reflection occurs for angles greater than 79 deg, so no signals escape through the windows at angles greater than this. These predicted losses do not include additional loss due to window coatings, metallization, the window shade, or the electronically dimmable shades being installed in some new aircraft.

Based on the location of the Soli device with respect to the window, the extent of the beam in azimuth and elevation as projected outside the plane can be computed, under the assumption that the device is a point isotropic source and its emissions are projected through the window. As one example, consider a scenario where the Soli device is held in the hand of a passenger sitting in the window seat. The device is centered on the middle of the window, but one-half of a seat width (9”) in from the window. Figure 2 below shows the extent in elevation and azimuth of the projected beam that emanates through the window. The maximum extent of the projected beam out of the window reaches about +/-30 deg in azimuth, and about +/-40 deg in elevation. No appreciable emissions outside of those ranges would be created, as the plane’s fuselage blocks such emissions. The only significant emissions are those that radiate through the window, with effectively no diffraction outside of that geometry.

[4] Zodiac Aerospace, *Aircraft 60 GHz BRAN*, Presentation to European Conference of Postal and Telecomms. Admins. (CEPT) Short Range Devices Maintenance Group at 7-10 (Apr. 2016), *available at* https://cept.org/Documents/srdmg/30181/srdmg-16-024_60-ghz-onboard-airplanes.

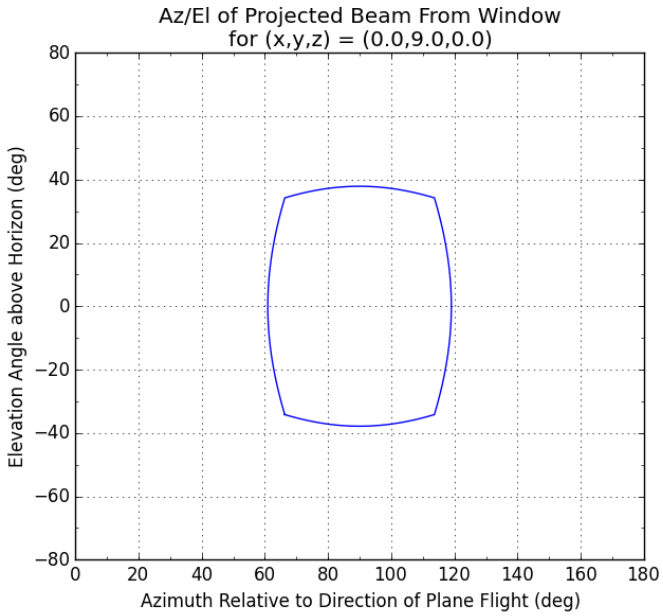

Figure 2: Projected beam of the Soli device's emissions outside of an airplane window, assuming the device is centered on the window and 9 inches inward of the window (i.e., in the hands of a user sitting in the window seat).

Another scenario is for the Soli device to be on the same passenger's lap, still about 9" in from the side of the plane, but 12" below the bottom of the window pane. Now the emissions are collimated into a smaller beam that exits the plane at a higher but narrower elevation range of about 50-70 deg.

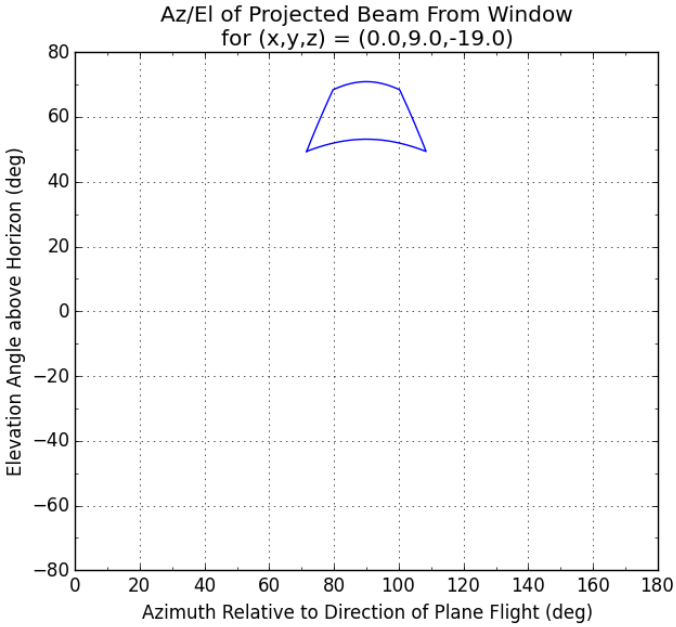

Figure 3: Projected beam of Soli emissions outside of an airplane window, assuming the device is centered on the window in the fore and aft direction, but 19 inches below the center of the window and 9 inches inward of the window (i.e., in the lap of a user in the window seat).

A third scenario is the device in the lap of a user sitting in the aisle seat, two seat widths (36") farther from the window. In that case, the projection of the Soli device's emissions out of the window is much more constrained, as shown in Figure 4.

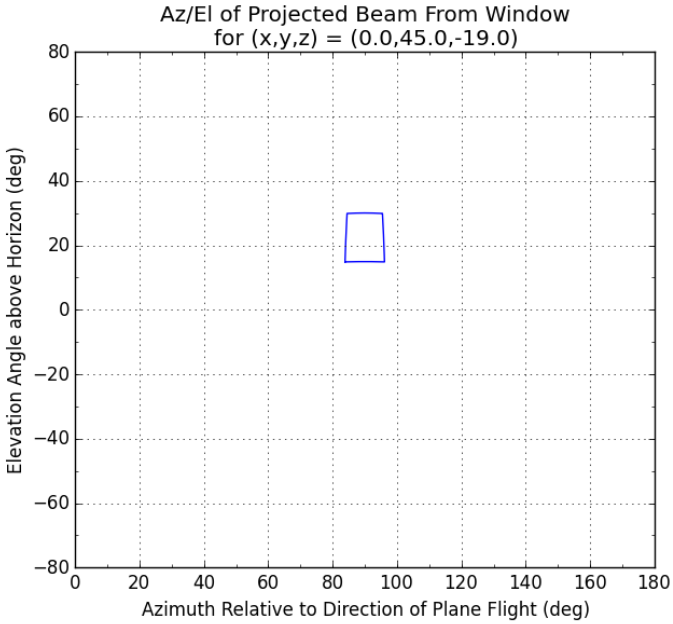

Figure 4: Projected beam of the Soli device's emissions outside of an airplane window, assuming the device is centered on the window in the fore and aft direction, but 19 inches below the center of the window and 45 inches inward of the window (i.e., in the lap of a user in the aisle seat for a plane with three seats on that side).

The geometry of the Soli device location and its projected beam out of the window is important because it demonstrates that under almost any normal situation, the Soli device will not emit radiation out of the window directly up into the sky (i.e., at an elevation angle of 90 deg). In a reasonably worst-case situation (Figure 3), the emissions may reach an elevation angle of about 70 deg.[5] Under other situations (i.e., Figures 2 and 4), the emissions will be much more constrained in elevation, not reaching above 40 deg in those examples.

This result impacts the analysis substantially, in two ways:

1. The known sensor systems operating in the band are scanning instruments that scan to a maximum angle of 48.3 deg (AMSU-A[6]) or 52.8 deg (ATMS[7]) as measured from the

[5] As noted previously, regardless of geometry, total internal reflection is expected to occur at angles greater than 79 deg, so no emissions at all will be emitted at angles greater than this value.
[6] Nat'l Oceanic and Atmospheric Admin. (NOAA), *Digital Earth Emissivity Information System (DEEIS) - Instruments: AMSU-Overview*, at https://www.star.nesdis.noaa.gov/smcd/spb/LANDEM/instr_AMSU.php (NOAA *DEEIS*: *AMSU*).
[7] Curtis Allmon and Dave Putnam, *Design of the ATMS Scan Drive Mechanism*, Proceedings of the 38th Aerospace Mechanisms Symposium (May 2006), *available at* http://www.esmats.eu/amspapers/pastpapers/pdfs/2006/allmon.pdf.

point directly below the satellite. The SSMIS instrument scans at a constant angle of 45 deg.[8] Because of this beam pointing geometry, emissions emanating from a plane window at elevation angles no greater than the complementary angle (i.e., 90 deg minus the beam scan angle), about 41 deg for AMSU-A and 37 deg for ATMS, will not point into a sensor beam (absent significant banking of the aircraft, which is infrequent at cruising altitude), and will therefore not cause interference. For SSMIS, *only* signals emitted from the plane at a slant path of 45 deg will point into the beam. Roughly speaking, devices used by occupants of aisle seats, and devices used by occupants of middle seats when the device is held above their laps, will therefore not create emissions outside of the plane that can interfere into a sensor beam.

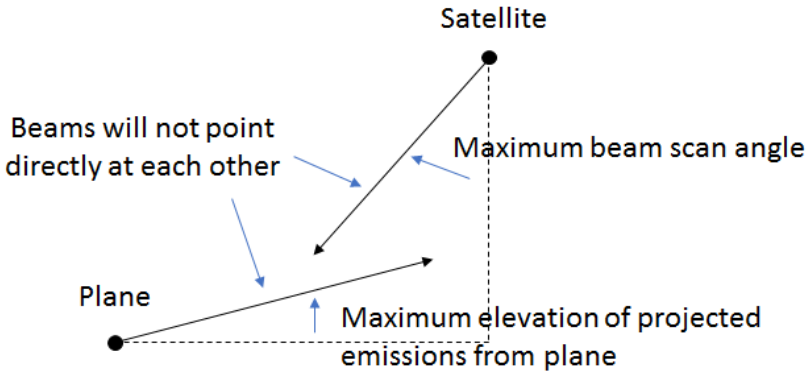

Figure 5: Geometry showing example of when satellite sensor beam and emissions emanating out of an airplane window will not point directly towards one another.

2. When emissions could potentially point into a sensor beam, they will do so only on slant paths through the atmosphere. The lower this slant path is in elevation, the greater the distance through the atmosphere that it must travel. The longer path will result, approximately, in proportionately more atmospheric attenuation. The result is that these interfering paths will be less problematic than the "straight-up" path assumed in some calculations (i.e., the basic calculations presented by CORF). Signals into SSMIS will always be on a 45 deg slant path due to the satellite's fixed scan geometry.

[8] NOAA, *Special Sensor Microwave Imager and Sounder (SSMIS) Antenna Brightness Temperature Data Record (TDR) Calibration and Validation User Manual* (Mar. 2007), *available at* ftp://rain.atmos.colostate.edu/FCDR/doc/SSMIS_general/NOAA_STAR_SSMIS_TDR_CalVal_User_Manual.pdf.

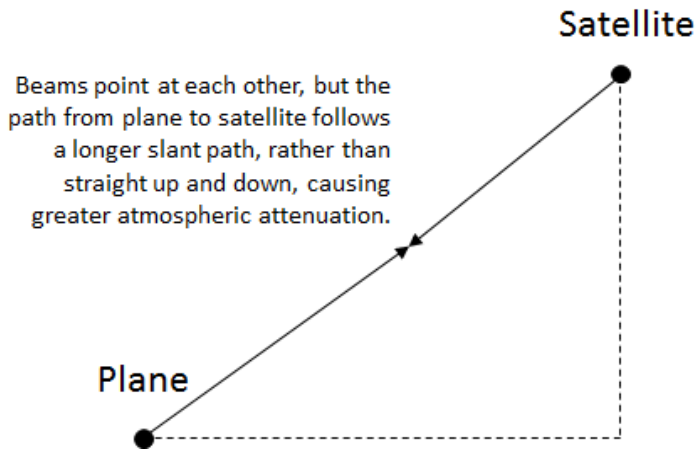

Figure 6: Geometry showing example of when satellite sensor beam and emissions emanating out of an airplane are able to point directly at one another. However, in this case, the path from airplane to satellite must follow a slant (diagonal) path, creating a longer distance through the atmosphere and Therefore greater atmospheric attenuation compared to a straight up/down path.

2.3 Atmospheric Attenuation between Airplane and Satellite

Given the foregoing geometric considerations, increased attenuation on the slant path from plane to satellite must be taken into account when computing the amount of interference incident upon the satellite sensor.

In the plausible scenario with increased high-elevation emissions out of an aircraft window (i.e., a Soli device sitting on the lap of a passenger in the window seat), the maximum elevation angle of the interference emanating from a plane is estimated to be approximately 70 deg. According to the Zodiac Aerospace study, total internal reflection from the acrylic window panes limits the elevation angle to no more than 79 deg. For analysis, the 79 deg absolute worst-case angle will be assumed.

Figure 7 shows the attenuation to space as a function of frequency across the 57.5 to 63.5 GHz frequency range used by Soli technology, from an altitude of 40,000 ft. The loss is computed using the *am* atmospheric model[9] (the same model used by CORF) with 1 MHz frequency steps, and assuming a 79 deg elevation angle with respect to the horizon.

[9] *See* Scott Paine, *The am Atmospheric Model*, Submillimeter Array (SMA) Technical Memo #152 (Mar. 2018), *available at* https://doi.org/10.5281/zenodo.1193646. The northern midlatitude annual atmospheric layer model was used. *See* Scott Paine, *am Atmospheric Model: am Cookbook*, Harvard-Smithsonian Center for Astrophysics, at https://www.cfa.harvard.edu/~spaine/am/ (last visited June 8, 2018) (providing the files for the northern midlatitude annual atmospheric layer model).

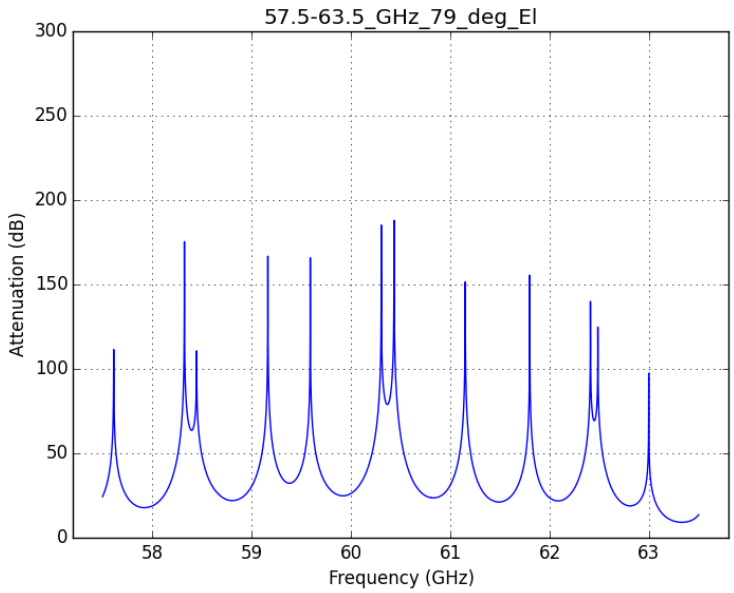

Figure 7: Attenuation to space from 40,000 ft assuming an elevation angle of 79 deg, i.e., worst-case to AMSU-A and ATMS.

Figure 8 shows the attenuation that occurs on a 45 deg slant path, which always applies to SSMIS. Because of the longer path through the atmosphere, attenuation into SSMIS is always much larger than the potential interference into AMSU-A and ATMS. (Note that the 45 deg slant path distance to SSMIS, which orbits at 850 km, is 1122 km, so the free space loss to SSMIS will be about 3 dB greater than for the 79 deg slant path to the AMSU-A and ATMS sensors at 820 km).

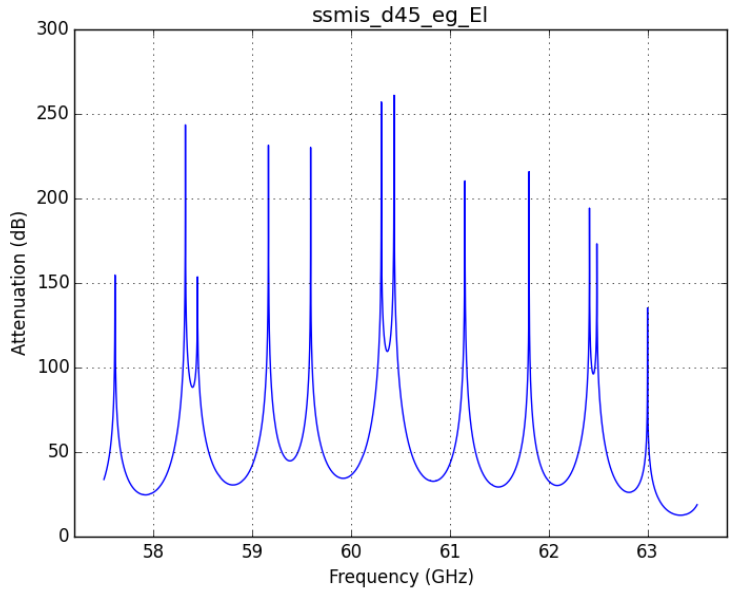

Figure 8: Attenuation to space from 40,000 ft assuming an elevation angle of 45 deg, i.e., the only path to SSMIS.

The attenuation for each sensor channel is computed by convolving the atmospheric attenuation profile over the channel bandwidth (assuming infinite attenuation for frequencies that are outside of the Soli device's sweep range). For example, channel 7 of the SSMIS sensor has a nominal frequency range of 59.2805 to 59.5195 GHz (239 MHz bandwidth), with a frequency stability factor of 10 MHz. The atmospheric attenuation curve in this range shows slightly less attenuation at the lower end of channel 7's range, so the minimum attenuation (greatest interference) for channel 7 is computed when the channel is 10 MHz lower in frequency than its nominal value, 59.2705 to 59.5095 GHz, over which the atmospheric attenuation is computed by convolving the data in Figure 8 to be 47.5 dB.

2.4 Greatest Interference Power

This section derives the worst-case interference to each sensor based on the combined effects of atmospheric attenuation (Section 2.3) and bandwidth overlap (Section 2.1).

The interference power into each sensor channel from a Soli device depends on several factors. First, the amount of overlap between the Soli sweep range and the sensor channel's frequency range impacts the effective EIRP, as noted in Section 2.1. Second, the amount of atmospheric attenuation over the channel's frequency range determines how much transmitted power makes it through the atmosphere to the satellite, as discussed in Section 2.3. Third, the total impact of a Soli device on the sensor channel depends on the combination of the two factors. Fourth, most channels have variable offsets and frequency stability factors, and the total impact (i.e., the effective EIRP minus atmospheric attenuation) will vary over the total tunable range of the channel, potentially in a complex manner that takes into account the bandwidth overlap and the complex shape of the attenuation curve with frequency.

To determine the greatest coupling between interference generated by aSoli device and a satellite sensor, every possible frequency range of each channel was varied (in 1 MHz increments), and the overlap bandwidth and atmospheric attenuation were computed for each possible range. For each channel, the worst-case combined factor was determined.

For example, consider AMSU-A channel 11. The nominal center frequency of this channel is 57.290344 GHz, with a 36 MHz bandwidth, giving a channel range of 57.272344 to 57.308344 GHz. This nominal channel range is below the Soli sweep range of 57.5 to 63.5 GHz, so there would be no interference. However, channel 11 has a maximum frequency offset of 370.2 MHz and a stability of 1.2 MHz. Therefore, the center frequency of the channel could be as high as 57.290344 GHz + 370.2 MHz + 1.2 MHz = 57.661744 GHz, corresponding to a frequency range including the 36 MHz bandwidth of 57.643744 to 57.679744 GHz, which is entirely within the Soli sweep range. As evident from Figure 7, the atmospheric attenuation at the lowest end of the sweep range (57.5 GHz) increases with frequency. Therefore, all things considered, the maximum amount of interference from a Soli device into channel 11 occurs when: (1) the frequency offset is just large enough that the channel is entirely within the Soli sweep range (to

maximize effective EIRP in accordance with Section 2.1), and (2) the channel is at the very lowest frequency that puts it entirely within the Soli sweep range so as to minimize atmospheric attenuation. When channel 11 is tuned to 57.5 to 57.536 GHz, maximum interference power into AMSU-A channel 11 is realized.

The following table summarizes the results of the above analysis for each channel of each sensor. The results have been rounded to 1 MHz.

Table 1: Worst-Case Interference Scenario for Each Sensor Channel

Sensor	Channel	Worst-Case (Greatest Interference) Bandwidth Overlap Correction + Atm Atten				
		Worst-Case Frequency Range (MHz)	Soli Overlap Bandwidth (MHz)	Overlap Correction Factor (dB)	Atm. Atten. (dB)	Overlap Correction + Atm Atten.
AMSU-A	10	57500 - 57545	45	-21.2	-27.2	-48.5
AMSU-A	11	57500 - 57536	36	-22.2	-26.6	-48.8
AMSU-A	12	57500 - 57516	16	-25.7	-25.3	-51.0
AMSU-A	13	57500 - 57508	8	-28.8	-24.8	-53.5
AMSU-A	14	57500 - 57503	3	-33.0	-24.5	-57.5
ATMS	11	57500 - 57545	45	-21.2	-27.2	-48.5
ATMS	12	57500 - 57536	36	-22.2	-26.6	-48.8
ATMS	13	57500 - 57516	16	-25.7	-25.3	-51.0
ATMS	14	57500 - 57508	8	-28.8	-24.8	-53.5
ATMS	15	57500 - 57503	3	-33.0	-24.5	-57.5
SSMIS	7	59270 - 59509	239	-14.0	-47.5	-61.5
SSMIS	19	63332 - 63333	1	-37.8	-12.6	-50.4
SSMIS	20	60831 - 60832	1	-37.8	-32.7	-70.5
SSMIS	21	60831 - 60832	1	-37.8	-32.7	-70.5
SSMIS	22	60831 - 60833	2	-34.8	-32.7	-67.5
SSMIS	23	60828 - 60835	7	-29.3	-32.7	-62.0
SSMIS	24	60819 - 60845	26	-23.6	-32.7	-56.4

The worst-case (least total attenuation) result among all channels and all sensors is AMSU-A channel 10 and ATMS channel 11, each with a total bandwidth overlap of 45 MHz out of the 78 MHz channel, resulting in a worst-case bandwidth correction factor + atmospheric attenuation of -48.5 dB.

2.5 Number of Soli Devices Contributing to Interference

While the number of Soli devices that actually would be in active use aboard an airplane is difficult to predict, for the sake of calculation it is conservatively assumed that 10% of the passengers are actively using Soli-enabled devices at the same time. As explained in Section 2.2, only devices in use in about half the seats (window and some middle seats) will contribute to the potential interference. Devices associated with 5% of the passengers would be contributors under these conditions. Assuming an average passenger load of 200, the number of passengers per flight using Soli devices simultaneously would be approximately 200 * 5% = 10. Therefore, an approximate multiple exposure factor is 10 log10(10) = 10 dB.

The number of planes in a single sensor beam at one time can be estimated based on the average spatial density of flights and the spatial dimensions of the sensor beam. Using actual flight data (see Section 4), the greatest number of flights in the air over the U.S. (or within 500 km of the border) at one time in the preceding year was 6342, of which 2339 were at a flight level of 30,000 ft or greater (i.e., high enough to potentially affect EESS sensors).[10] The total area encapsulating these flights was 23,048,437 km^2, so that the average surface density of the planes was $1.0x10^{4}$ km^{2}. The AMSU-A instrument has the largest beamwidth, at 3.3 deg. From an orbit of 820 km, this corresponds to a beam area of approximately 1855 km^2. Therefore, the average number of planes per beam under this scenario is $1.0x10^{4}$ km^{2} x 1855 km^2 = 0.19. While there is some spatial clustering of flights along major flight routes and near airports (although flights near airports are at much lower altitude), the estimated number of flights per beam is conservative, because the worst single hour flight density for the preceding year is used and it is assumed that flights as low as 30,000 ft could impact an EESS sensor, when in fact atmospheric attenuation to space at that altitude is considerably larger than the values discussed in Section 2.3. Nonetheless, one plane per sensor beam, which is more than five times greater than the estimate above, is assumed here.

2.6 EESS Sensor Antenna Gain

According to the data and references in Appendix A, the antenna gain for AMSU-A is approximately 36 dBi, for ATMS is approximately 40 dBi, and for SSMIS approximately 50 dBi.

2.7 Protection Criterion for EESS Sensors

According to ITU-R Recommendation RS.2017,[11] the interference criterion for passive EESS sensors operating in the 57 GHz band is -139 dBm in 100 MHz, not to be exceeded for more than 0.01% of the time.

---

[10] *See* Flightradar 24.com at https://www.flightradar24.com/ (a global tracking service that provides real-time and historical information about flights) (last visited June 8, 2018).
[11] Int'l Telecomm. Union, *Performance and Interference Criteria for Satellite Passive Remote Sensing*, Recommendation ITU-R RS.2017-0 at 5 (Aug. 2012), *available at* https://www.itu.int/dms_pubrec/itu-r/rec/rs/R-REC-RS.2017-0-201208-I!!PDF-E.pdf (ITU-R RS.2017-0).

2.8 Total Interference to EESS Sensors

Based on the foregoing considerations, the total interference to EESS sensors from airborne use of Soli devices can be estimated, assuming worst case (i.e., AMSU-A channel 10 and ATMS channel 11):

Item	**Value**
Soli device EIRP	13 dBm (20 dBm)[12]
Duty cycle factor	-10 dB
Worst-case frequency overlap correction factor + atmospheric attenuation	-48.5 dB
Free space loss to 820 km orbit	-186 dB
Multiple exposure factor	10 dB
Antenna gain (ATMS)	40 dBi
Total power into sensor	**-181.5 dBm (-174.5 dBm)**
ITU-R interference criterion in 78 MHz channel @ -139 dBm/100 MHz	-140.1 dBm
Worst-case interference margin	**41.4 dB (34.4 dB)**

3. How the Results Differ from CORF's Approximate Calculations

CORF employed a number of assumptions in its approximate calculations that were generally even more conservative than the treatment provided here. The main differences are the following:

1. CORF assumed an EIRP for a Soli device of 20 dBm.[13] The actual maximum EIRP for Soli devices using currently available hardware components is approximately 13 dBm.

2. When considering bandwidth overlap and duty cycle factors with respect to the EESS sensors' integration times, the effective EIRP is 20 dB (or more) below the maximum (i.e., less than -7 dBm).

3. CORF assumed that propagation was "straight up" from the aircraft to the satellite. This path does not exist due to the geometry of the Soli device with respect to the aircraft

[12] Using currently available equipment, the measured EIRP of a Soli device is 13 dBm. Google requests permission to operate Soli devices at up to 20 dBm, for harmonization with European limits and to create flexibility for further advancements in development of Soli technology. The interference margin calculation in the final row of this table reflects both power levels.
[13] CORF Comments at 5, 7.

windows from which the emissions are able to pass through to the outside of the plane, as shown in Section 2.2 above. Also, based on total internal reflection, the maximum elevation angle to the satellite would be 79 deg. For SSMIS, the maximum angle to the sensor is 45 deg due to the fixed sensor scan angle.

4. CORF assumed 13 dB of atmospheric loss from an aircraft at 40,000 ft.[14] In the frequency range of 57.2 to 57.3 GHz, this value is approximately the correct *minimum* value based on the simulations herein, assuming that the signal travels straight up through the atmosphere. However, Soli technology does not operate in this frequency range. Its lowest frequency is 57.5 GHz, where the minimum attenuation on the same "straight-up" path is approximately 24 dB, or 9 dB greater than the value used by CORF. On a 79 deg slant path, the attenuation is about 25 dB.

4. General Compatibility of Soli Devices with EESS in the 57.5 to 63.5 GHz Band

The foregoing discussion is specific to known EESS sensors operating in and around the 57 GHz passive EESS allocation. Here, generic consideration is given to any other existing sensors and to potential future EESS sensors that may or may not have similar characteristics to the sensors examined above. Without access to specific operational criteria provided by the remote sensing community, the ability to conduct compatibility studies is extremely limited. The following discussion nevertheless attempts to extend the compatibility discussion in the context of generic protection criteria in ITU-R RS.2017, while reducing the number of assumptions regarding the EESS sensors themselves.

First, the EESS passive allocation extends to 59.3 GHz, while Soli operates only above 57.5 GHz. Therefore the protected overlap is at most 1.8 GHz of Soli's 6 GHz sweep range, so the fraction of time that Soli technology is within the protected range is 1.8/6 = 30%. Combined with Soli technology's maximum duty cycle of 10% that is assumed here, the EIRP within the protected band is, at most, 20 dBm * 30% * 10% = 4.8 dBm (assuming the maximum EIRP requested by Google).

Second, future sensors could use narrowband modes, in which case the minimum attenuation across the passband could be a relevant factor, as opposed to the integrated attenuation across the passband. Simulations show that in a 1 MHz channel, the minimum atmospheric attenuation on a 79 deg elevation angle is approximately 17.8 dB (near 57.9 GHz). (For the worst-case "straight-up" path, the minimum attenuation is ~17.5 dB in 1 MHz, and ~17.6 dB over 100 MHz.) However, when considering narrowband channels, the bandwidth reduction factor becomes more significant, and the effective EIRP is reduced proportionately. For example, with a 1 MHz channel and assuming a 10% duty cycle for Soli, the effective EIRP is equal to 20 dBm * (1 MHz/6 GHz) * 10% = -27.8 dBm, due to both the pulse duty cycle and the fraction of time the

[14] CORF Comments at 5.

chirped signal spends within a 1 MHz channel. The exact factors will depend on the nature of the EESS sensor, including the channel bandwidth and effective integration time.

Using these considerations, it is possible to compare a worst-case interference amplitude for a 100 MHz portion of the band into a satellite receiver, against the ITU-R RS.2017-0 criterion.[15] The effective Soli EIRP would be 20 dBm * 10% * (100 MHz/6 GHz) = -7.8 dBm. The worst-case ("straight-up") atmospheric attenuation across 100 MHz is approximately 17.6 dB from 40,000 ft. The free space loss is an additional 186 dB. The received interference power at the satellite would be -7.8 dBm - 17.6 dB - 186 dB = -211.4 dBm, which is 72.4 dB below the ITU-R RS.2017-0 protection level of -139 dBm per 100 MHz.[16] Even with a 40 dBi sensor antenna, and a 10 dB multiple exposure factor, the received power at the sensor is still some 22.4 dB below the interference criterion. Realistic paths (i.e., slant paths as discussed in Section 2.2) would have even greater margins.

Similarly illuminating is an analysis of the integrated interference reaching an EESS sensor from all aircraft simultaneously. Based on flight data for the twelve month period from April 2017 to March 2018, and taking into account every aircraft traveling within 500 km of the contiguous United States, the typical number of flights in the air during the busiest hour of the day is approximately 5000, but occasionally more due to high travel demand.[17] During this one-year period, the busiest month was August 2017 and the busiest day was August 21, 2017. Based on a snapshot of flight data taken at 30 minutes past every hour, the busiest hour was August 21, 2017, at 19:00-20:00 UTC. This date and time is shortly after the total solar eclipse that passed across the U.S., which resulted in an unusually high count of aircraft, reaching 6432 planes in the air over the U.S. during that hour. The histogram of flight altitudes during this snapshot is shown in Figure 9.

[15] *See supra* note 11.
[16] *Id.*
[17] Data used for calculations in this section were derived from flightradar24.com. *See* Flightradar24.com at https://www.flightradar24.com/ (last visited June 8, 2018).

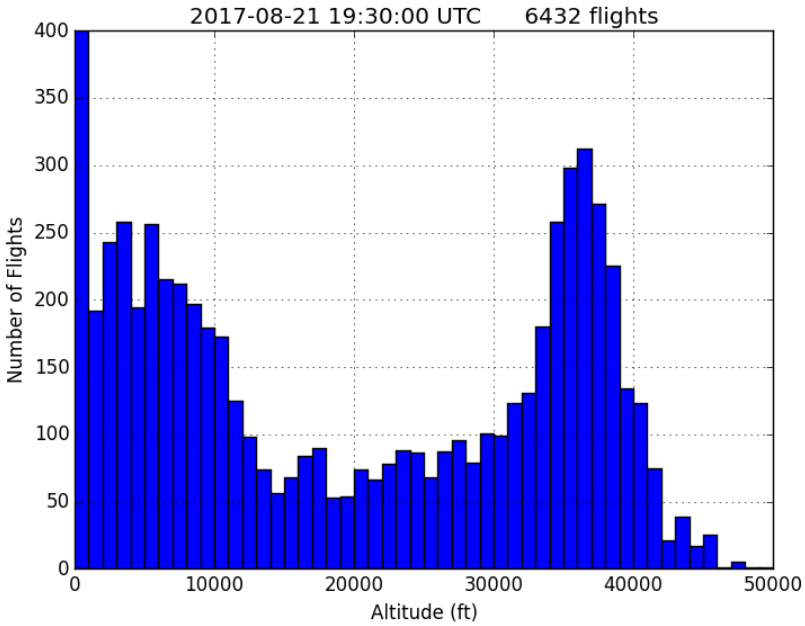

Figure 9: Distribution of flights by altitude during the busiest single hour of the preceding year.

The flight histogram can be combined with atmospheric attenuation as a function of altitude to create the worst possible case of an EESS sensor being exposed to every flight over the U.S. simultaneously. In that case, the sensor's antenna would have to be sensitive to the entire hemisphere below it, so that all of the planes are in the beam at one time (it is physically impossible to have high antenna gain and broad coverage at the same time). Therefore, the antenna would have a gain of about 3 dB (hemispherical coverage). The differential contribution at each flight altitude h is:

$$dI(h) = -7.8\ \text{dBm} + 10\log10[N(h)] - A(h) - FSL(h) + MEF + G,$$

where

- dI(h) is the differential contribution to the total interference in a 100 MHz bandwidth from all flights at altitude h,
- -7.8 dBm is the EIRP of a single Soli device across 100 MHz,
- N(h) is the number of flights at altitude h (as specified by the histogram in Figure 9),
- A(h) is the minimum atmospheric attenuation integrated over a 100 MHz bandwidth from height h to space (see Figure 10),
- FSL(h) is the free space loss from height h to a satellite directly overhead at an altitude of 820 km,
- MEF is a multiple exposure factor, here taken to be 10 dB, per section 2.5, and
- G is the EESS sensor antenna gain, taken to be 3 dB.

The total interference is the integral of dI(h) over all h from 0 to 50,000 ft (which is the highest flight altitude seen in the data, except for a very small number of specialized aircraft and balloons).

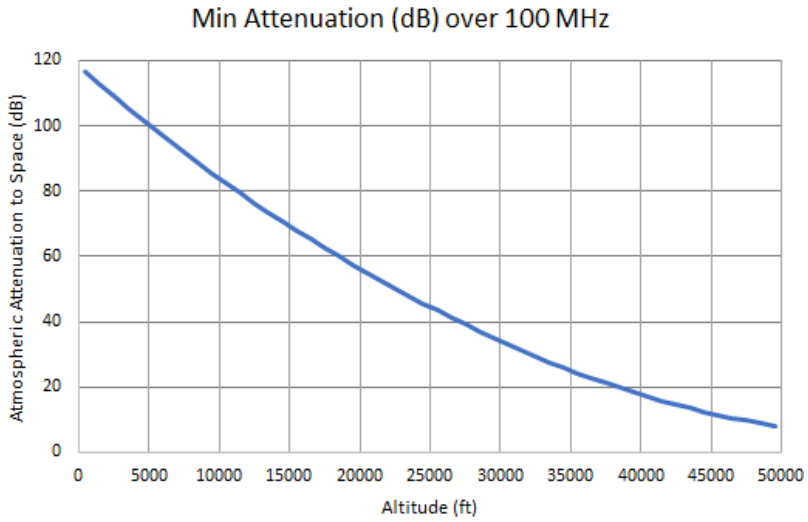

Figure 10: Minimum ("straight up") atmospheric attenuation to space integrated over a 100 MHz bandwidth.

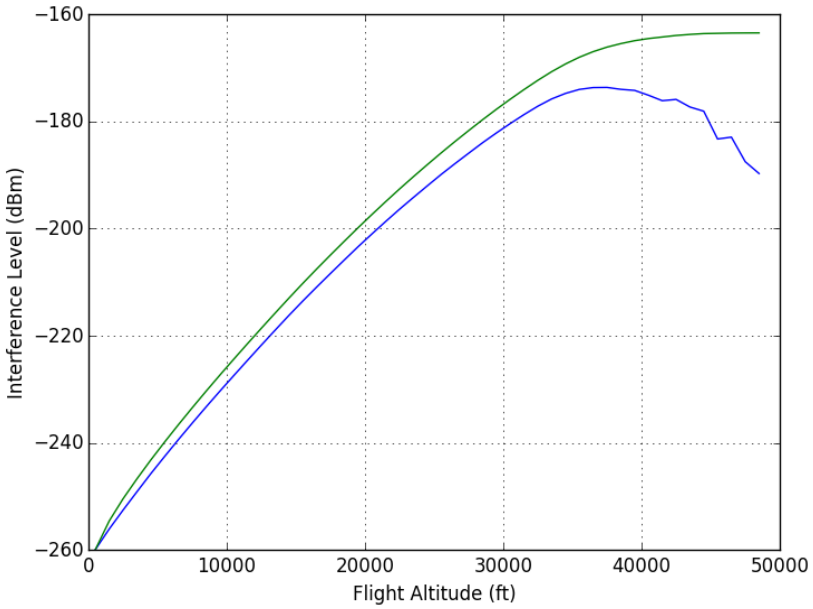

Figure 11: The blue line shows the contribution (dI) to total interference from each individual height (in 1000-ft increments) due to the distribution of flights in Figure 9 combined with the attenuation in Figure 10; the green line shows the cumulative interference from all flights at or below a given altitude. Considering every flight in the air (up to 50,000 ft), the total interference during the busiest single hour of the year would be about -163.5 dBm, some 24.5 dB below the EESS interference criterion.

Based on the formula above and the actual flight data during the snapshot taken during the busiest hour of the preceding year, the total integrated interference from every aircraft in flight

over the U.S., across the entire EESS (passive) allocation, to a single EESS sensor would be -163.5 dBm, which is 24.5 dB below the EESS interference criterion of -139 dBm. Although this is a somewhat unphysical case (even a hemispherical antenna could not see the entire U.S. land area from 820 km orbit), it demonstrates that there is wide margin to meet the EESS interference requirements, even considering every plane in the sky.

5. Additional Factors Not Included in the Margin Calculation

To reiterate points made above, at least two relevant factors have not been included in the foregoing calculations. The first is the attenuation out of the airplane windows, which was predicted by Zodiac Aerospace to be 11.6 dB, based on reflectivity and transmission characteristics of the acrylic components.

Second is the radiation pattern of the Soli device. Throughout, it has been assumed that the Soli device emits equally in all directions. In reality, the emissions are concentrated toward the front of the device, with lower levels of emissions toward the sides and back of the device. The impact to the analysis here is that even lower levels of Soli emissions would be present toward the airplane windows.

6. Conclusions

Employing reasonable, albeit conservative, assumptions shows that airborne use of Soli devices will protect existing EESS sensors with a margin of over 30 dB. The main factors contributing to the wide margin are the low maximum EIRP of a Soli device, the duty cycle of the Soli emissions, the bandwidth overlap factor between the EESS sensor channel and the Soli sweep range, and atmospheric attenuation. A worst-case analysis against future EESS sensors whose specific operating characteristics are not publicly available shows a likely interference margin of at least 22 dB using generic ITU-R Rec RS.2017 criteria.

All interference margins would be increased by more than 11.6 dB (i.e., to more than 40 dB for known sensors and to more than 30 dB for the generic case) taking into account the attenuation of the airplane windows and the beam pattern of the Soli emissions.

Appendix A
Characteristics of Satellites and Sensors Potentially Affected

The following potentially affected EESS sensors are included in this analysis. The satellites on which they fly are listed, along with their altitude above the Earth's surface.

Table A-1: EESS Sensors & Satellites

Sensor	Satellites	Altitude (km)
AMSU-A[18]	NOAA-15 NOAA-16 NOAA-18 NOAA-19 Aqua (NASA) Metop-A (EUMETSAT) Metop-B (EUMETSAT) Metop-C (EUMETSAT)[19]	810 847 855 864 701 820 822 817
ATMS[20]	Suomi-NPP JPSS-1/NOAA-20 JPSS-2[21]	834 833 833
SSMIS[22]	DMSP F16 DMSP F17 DMSP F18 DMSP F20[23]	850

The following table derives the maximum total range of frequencies over which the sensors may operate. The lowest and highest possible value of each sensor's channel edges are derived for each channel of the sensor that falls, or may fall, within Soli's sweep range. Each channel has a nominal center frequency, a maximum offset of the center frequency from the nominal value, a frequency stability, and a bandwidth. The lowest and highest channel edge frequencies are derived from all of these factors combined. The minimum and maximum channel edges are only used to compute the extent to which the channel could overlap with the Soli sweep range. The actual channel bandwidth is always equal to the bandwidth listed in the table; that is, the lowest

[18] World Meteorological Org. (WMO) Observing Systems Capability Analysis and Review Tool (OSCAR), *Instrument: AMSU-A,* https://www.wmo-sat.info/oscar/instruments/view/30 (last visited June 8, 2018) (OSCAR *AMSU-A*).
[19] Not yet launched.
[20] WMO OSCAR, *Instrument: ATMS*, https://www.wmo-sat.info/oscar/instruments/view/53 (last visited June 8, 2018) (OSCAR *ATMS*).
[21] Not yet launched.
[22] National Snow and Ice Data Center (NSIDC), *Special Sensor Microwave Imager/Sounder (SSMIS)*, https://nsidc.org/data/pm/ssmis_instrument (last visited June 8, 2018) (NSIDC *SSMIS*).
[23] Not yet launched.

and highest channel edges are not the extent of the received bandwidth, only the least and greatest frequency that could be within the channel's bandwidth given the factors above.

Table A-2: EESS Sensor Channels Possibly within Soli Sweep Range

Sensor	Channel	Channel Bandwidth (MHz)	Maximum Range of Channel Edges Including Frequency Offsets, Frequency Stability, and Channel Bandwidth (GHz)	
			Lowest	Highest
AMSU-A[24]	10	78	57.033844	57.546844
	11	36	56.900944	57.679744
	12	16	56.936944	57.643744
	13	8	56.953644	57.627044
	14	3	56.961544	57.619144
ATMS[25]	11	78	57.033844	57.546844
	12	36	56.901844	57.678844
	13	16	56.937844	57.642844
	14	8	56.953844	57.626844
	15	3	56.961644	57.619044
SSMIS[26]	7	239	59.2705	59.5295
	19	1.35	62.997222	63.569274
	20	1.35	60.434021	61.151315
	21	1.3	60.432046	61.15329
	22	2.6	60.427896	61.15744
	23	7.35	60.415021	61.170315
	24	26.5	60.371446	61.21389

[24] OSCAR *AMSU-A*.
[25] OSCAR *ATMS*.
[26] NSIDC *SSMIS.*

Table A-3: Sensor Antenna Beam and Scan Pattern Characteristics

Sensor	Beam Size & Approximate Gain	Min/Max Field of View @ 57 GHz	Scan Period (s)	Integration Time (ms)
AMSU-A	3.3 deg/36 dBi[27]	Min: 48.6 x 48.6 km = 1,855 km^2 Max: 155.2 x 85.6 km = 10,434 km^2	8[28]	165 ms[29]
ATMS	2.2 deg/40 dBi[30]	Min: 31.6 x 31.6 km = 784 km^2 Max: 136.7 x 60 km = 6,442 km^2	2.667[31]	16 ms[32]
SSMIS[33]	0.72 deg/50 dBi	16 x 26 km = 326 km^2	1.9[34]	4.1 ms[35]

[27] Int'l Telecomm. Union, *Spectrum Sharing Between Spaceborne Passive Sensors and Inter-Satellite Links in the Range 50.2-59.3 GHz*, Recommendation ITU-R SA.1279 at 2 (1997), *available at* https://www.itu.int/dms_pubrec/itu-r/rec/sa/R-REC-SA.1279-0-199710-S!!PDF-E.pdf (ITU-R SA.1279).
[28] NOAA *DEEIS*: *AMSU*.
[29] *Id.*
[30] Fuzhong Weng (NASA), *Suomi NPP ATMS SDR Provisional Product Highlights* (Oct. 2012), *available at* https://www.star.nesdis.noaa.gov/jpss/documents/AMM/ATMS_SDR_Prov.pdf.
[31] Allmon and Putnam, *supra* note 7.
[32] *Id.*
[33] Northrop Grumman, *Algorithm and Data User Manual (ADUM) for the Special Sensor Microwave Imager/Sounder (SSMIS)*, July 29, 2002, *available at* ftp://rain.atmos.colostate.edu/FCDR/doc/SSMIS_general/Algorithm_and_Data_User_Manual_For_SSMIS_Jul02.pdf.
[34] *Id* at 4.
[35] *Id.*

Appendix B
Soli Device Characteristics

1. Frequency range: 57.5-63.5 GHz
2. Chirp type: Linear FM
3. Max EIRP: 13 dBm
4. Max EIRP PSD: 13 dBm (single CW tone linear FM sweep so power and power spectral density are equivalent)
5. Maximum duty cycle: 10%